
FINE-GRAINED TOKEN ALLOCATION VIA OPERATION PRUNING FOR EFFICIENT MLLMS

Aoming Liu
Boston University
amlu@bu.edu

Reuben Tan
Microsoft Research
tanreuben@microsoft.com

Boqing Gong
Boston University
bgong@bu.edu

Bryan A. Plummer
Boston University
bplum@bu.edu

ABSTRACT

Token reduction accelerates Multimodal Large Language Models (MLLMs) by reducing excessive tokens, but overlooks structural redundancy differences, where critical and redundant modules process identical token loads. For fine-grained computation control, we define an “operation” as the computation for a module to process a group of tokens and introduce the operation pruning framework to enable modules to selectively process tokens. Built on this framework, we propose **Depth-wise Operation Pruning (DOP)**, a data-driven method that searches for strategies to prune redundant operations and save computational budget for critical modules to process more tokens than uniform allocation by minimizing divergence from the original model’s output probability distribution on a small validation set while satisfying computational constraints. For efficient optimization, DOP applies depth-wise pruning to reduce policy space and uses an additive approximation to minimize required validation runs. Depth-wise pruning partitions operations by module type and token group, and prunes operations in deeper layers before those in shallower layers within each module-group pair. The additive approximation obtains individual divergences by independently varying each policy parameter, and then sums them to approximate the joint divergence of simultaneously changing all policy parameters, reducing required validation runs from exponential to linear with respect to the number of policy parameters. Comprehensive evaluations show that DOP establishes new state-of-the-art performance across 6 MLLMs and 13 benchmarks against 12 baselines. On LLaVA-Next-7B, DOP achieves 86% TFLOPS reduction and 83% latency reduction on real GPU with only 1% performance loss. Our extensive ablation studies further demonstrate DOP’s data and time efficiency as well as strong generalization capabilities.

1 INTRODUCTION

Multimodal Large Language Models (MLLMs) (Liu et al., 2024b;a; Li et al., 2023b; Team et al., 2023; Bai et al., 2023b; Chen et al., 2023b) face significant computational overhead primarily in their language model decoders (Achiam et al., 2023; Touvron et al., 2023; Peng et al., 2023; Abidin et al., 2024), which dramatically outweigh the lightweight visual encoders (*e.g.*, in LLaVA-1.5, 7B/13B decoder parameters versus 0.3B encoder parameters), due to excessive tokens increasing the computation in Multi-Head Attention (MHA) and Multi-Layer Perceptron (MLP) modules. As the majority of tokens are from visual input, reducing visual tokens is a common practice to accelerate MLLMs by reducing MHA/MLP computations, *e.g.*, token pruning methods (Li et al., 2024; Yao et al., 2024; Chen et al., 2024; Zhang et al., 2024c), built-in token reduction like resizing input images to smaller resolutions (Bai et al., 2025; Shi et al., 2025b). However, they often make all modules in the decoder process the same visual tokens, overlooking structural redundancy differences where certain modules contribute more critically to outputs than others.

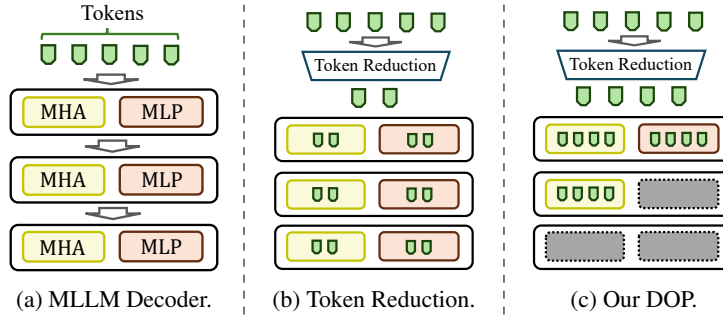


Figure 1: Comparison of our DOP and token reduction: (a) Computational overhead in MLLM decoders primarily stems from MHA and MLP modules processing excessive tokens. (b) Token reduction (Chen et al., 2024; Zhang et al., 2024a; 2025) has all modules process the same token load regardless of structural redundancy differences. (c) Our DOP prunes redundant operations and saves computational budget for critical modules to process more tokens than uniform allocation.

To achieve better performance-efficiency tradeoffs by allocating more tokens to critical modules and less for redundant ones, we introduce the operation pruning framework, where an “operation” is the computation for a module to process a group of tokens, and pruning means having that module selectively not process this group of tokens. Built on this framework, we propose **Depth-wise Operation Pruning (DOP)**, a data-driven method that prunes redundant operations with minimal impact on outputs and saves computational budget for critical modules to process more tokens than uniform allocation, as shown in Figure 1.

DOP optimizes pruning policies by minimizing divergence from the original model’s output probability distribution on a small validation set while satisfying computational constraints. For efficient optimization, DOP employs depth-wise pruning constraints and additive approximation. Depth-wise pruning reduces the policy space complexity from exponential to quadratic with respect to layer count by enforcing that operations for tokens in the same group within each module type (MHA or MLP) are pruned in depth order—deeper operations before shallower operations. Thus, a DOP policy for a single group of tokens consists of the token count within the group and the processing depth for each module type, where tokens are entirely excluded from each module type’s computation beyond that type’s specified depth. The optimization cost is further reduced by applying an additive approximation that replaces joint divergence with the sum of individual divergences from changing each policy parameter independently, reducing the required validation runs from exponential to linear with respect to the number of policy parameters.

Extensive experiments validate DOP as an effective, efficient, and versatile MLLM acceleration method through comprehensive evaluations across 6 different MLLMs, 13 benchmarks, and comparisons against 12 baselines. When only pruning visual operations, as all baselines only prune visual tokens, DOP consistently outperforms state-of-the-art baselines by preserving up to 7% more performance. Notably, on LLaVA-NeXT-7B, DOP reduces TFLOPs by 77% with no performance loss on average, and reduces TFLOPs by 86% with just 1% loss as well as 83% prefilling CUDA latency reduction. DOP is highly flexible and consistently improves performance with three different token reduction methods. Moreover, according to our ablation, DOP demonstrates both data efficiency, requiring as few as 25 validation samples and two minutes to optimize a good policy, and strong generalization capabilities, performing well when transferred to different tasks and models.

Our main contributions are summarized as follows:

1. We fundamentally extend MLLM acceleration beyond token reduction to fine-grained operation pruning, thereby enabling precise and fine-grained computation reduction via module-level token allocation based on both token redundancy and structural redundancy.
2. We propose Depth-wise Operation Pruning (DOP), an effective method for optimizing operation pruning policies, with depth-wise pruning constraints and additive approximation to make optimization extremely time- and data-efficient.
3. Our comprehensive evaluations and ablation studies show that DOP achieves state-of-the-art performance-efficiency tradeoffs with strong cross-task and cross-model generalization.

2 RELATED WORK

Token Reduction reduces MLLM (Liu et al., 2024b;a; Li et al., 2023b; Dai et al., 2023; Team et al., 2023; Bai et al., 2023a;b; Chen et al., 2023b; Liu et al., 2023a; Abdin et al., 2024; Lin et al., 2023b; Zhu et al., 2025; Bai et al., 2025) computation by reducing visual tokens to minimize the computation for MHA and MLP modules to process these tokens, with most being token pruning methods that directly discard redundant tokens (Chen et al., 2024; Zhang et al., 2024c; Lin et al., 2024; Ye et al., 2024; Zhang et al., 2024b; Yang et al., 2024; Xing et al., 2024; Alvar et al., 2025; Wen et al., 2025; Zhang et al., 2025), while others like token merging combine redundant tokens into critical tokens (Shang et al., 2024; Yang et al., 2024; Zhang et al., 2024c). Prior works mainly explore “what” tokens to prune by finding redundancy indicators. Early methods used LLM decoder attention (Chen et al., 2024; Zhang et al., 2024c; Ye et al., 2024; Xing et al., 2024), but later works noted position bias and switched to [CLS] attention (Zhang et al., 2024a; Yang et al., 2024; Shang et al., 2024) and feature diversity (Wen et al., 2025; Alvar et al., 2025). Recent CDPruner (Zhang et al., 2025) achieves state-of-the-art with conditional diversity. Additionally, many MLLMs have built-in token reduction like visual input resizing (Bai et al., 2025; Zhu et al., 2025; Shi et al., 2025a).

However, these methods rarely consider structural redundancy. Only a few progressive pruning works (Ye et al., 2024; Xing et al., 2024; Zhang et al., 2024c) explore this by allocating more tokens to shallower layers and fewer to deeper layers, performing well under loose budgets but poorly under tight budgets due to coarse-grained layer-level redundancy that overlooks module-level differences. For instance, a deeper MHA may be more critical than a shallower MLP. Additionally, progressive pruning has usage limitations like FlashAttention incompatibility or requiring redundancy ranking, limiting compatibility with diversity-based or resizing methods.

KV caching (Kwon et al., 2023) accelerates MLLM inference by reusing computed key-value pairs of processed tokens, dividing the inference process into a prefilling stage, where all tokens are fully processed to generate the first token, and subsequent decoding stages, where KV cache exempts certain DOP components (*e.g.*, MHA and MLP modules) from full-token processing. Our DOP primarily optimizes the prefilling stage, which aligns with prior token pruning approaches (Shang et al., 2024; Chen et al., 2024; Zhang et al., 2024c; Lin et al., 2024; Ye et al., 2024; Zhang et al., 2024b; Yang et al., 2024; Xing et al., 2024). Zhong et al. (2024) also confirms prefilling is compute-bound, while decoding is memory-bandwidth-bound, validating our focus on prefilling efficiency.

We discuss additional related work in Section B, including MLLM architectures and the distinction between DOP and Neural Architecture Search.

3 DEPTH-WISE OPERATION PRUNING

We aim to eliminate redundant MLLM computations while minimizing the performance impact. We target the parameter-dense decoder ($20\times$ larger than the visual encoder) during the compute-bound prefilling stage (Zhong et al., 2024), following Shang et al. (2024); Chen et al. (2024); Yang et al. (2024), by decomposing computation into operations and pruning the most redundant ones.

To formalize this approach, we first provide a general formulation without introducing specific settings. Let \mathbf{o} denote an operation and $\mathcal{O} = \{\mathbf{o}_1, \mathbf{o}_2, \dots\}$ denote the set of all operations, where each operation is the computation for an MHA/MLP module to process a group of tokens. Then, operation pruning is represented as $\mathcal{O} \setminus \mathcal{P}$, where any subset $\mathcal{P} \subseteq \mathcal{O}$ can be a pruning policy. We aim to find the optimal policy \mathcal{P}^* that maximizes performance while meeting computation constraints. Given τ as the maximum computation allowed, the pruning policy optimization is:

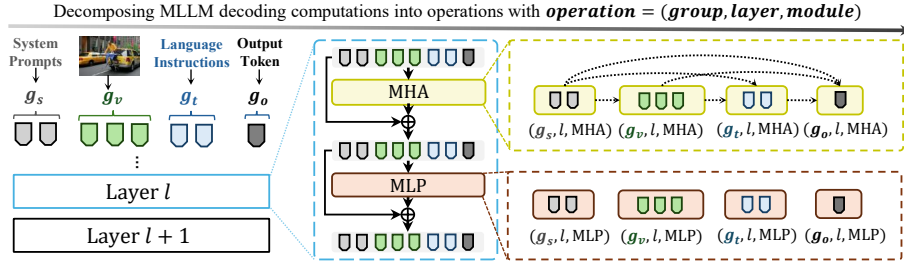
$$\mathcal{P}^* = \arg \max_{\mathcal{P} \subseteq \mathcal{O}} \text{Performance}(\mathcal{O} \setminus \mathcal{P}) \quad \text{s.t.} \quad \text{Computation}(\mathcal{O} \setminus \mathcal{P}) \leq \tau \quad (1)$$

Section 3.1 below will concretize the operation pruning framework with analysis, while Section 3.2 introduces our optimization details for the pruning policy.

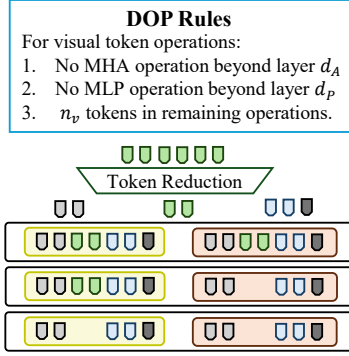
3.1 OPERATION PRUNING FRAMEWORK

As shown in Figure 2a, we decompose MLLM decoder computations along three dimensions into atomic operations: token groups, layer positions, and modules. Each operation is defined as:

$$\mathbf{o} = (g, l, m), \quad \mathbf{o} \in \mathcal{O} = \mathcal{G} \times \mathcal{L} \times \mathcal{M}. \quad (2)$$

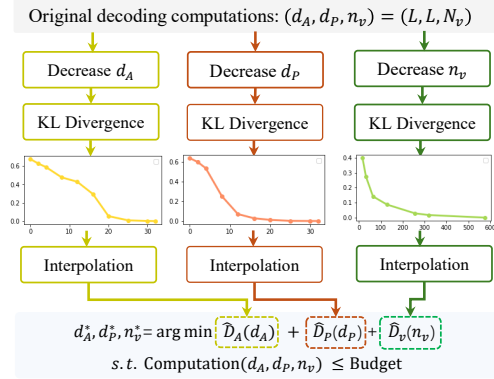


(a) Decompose MLLM decoder computations into operations.



DOP with $(d_A, d_P, n_v) = (2, 1, 2)$

(b) DOP Policy Illustration.



(c) DOP Policy Optimization.

Figure 2: **Overview of DOP.** (a) DOP decomposes MLLM decoder computations into operations defined by $(group, layer, module)$ as atomic computation carriers. Tokens are categorized into four groups based on input sources, and we prune operations for the visual token group in MHA and MLP modules. (b) DOP employs depth-wise pruning: visual tokens bypass MHA operations beyond layer d_A and MLP operations beyond layer d_P , with remaining operations processing n_v selected visual tokens. (c) DOP reduces optimization cost through additive approximation by replacing joint divergence with the sum of individual divergences measured by independently reducing d_A , d_P , n_v and computing respective KL divergences from original model’s output probability distribution. Evaluation points are sparsely sampled, with other points obtained through interpolation.

Each operation (g, l, m) represents the computation for the m module in layer l to process the tokens in group g . \mathcal{O} is the set of all operations, $\mathcal{G} = \{\mathbf{g}_s, \mathbf{g}_v, \mathbf{g}_t, \mathbf{g}_o\}$ is the set of token groups based on their sources: system, visual, text, and output, respectively, $\mathcal{L} = \{1, \dots, L\}$ represents the set of layer indices, and $\mathcal{M} = \{MHA, MLP\}$ is the set of module types. These are detailed below.

Token Groups. DOP groups tokens to avoid excessive operations from token-by-token division, reducing optimization cost. We categorize tokens into four groups based on input sources: \mathbf{g}_s from system prompts, \mathbf{g}_v from visual inputs, consisting of n_v critical visual tokens selected through existing visual token reduction methods (Zhang et al., 2024a; 2025), \mathbf{g}_t from language instructions, and output tokens \mathbf{g}_o . While our framework supports pruning operations for all four groups, we primarily focus on pruning operations for visual tokens \mathbf{g}_v due to their prevalence and for fair comparison with baselines only pruning visual tokens (Chen et al., 2024; Zhang et al., 2024a; 2025).

Visual Token Reduction. To get the visual token group \mathbf{g}_v , we employ existing visual token reduction methods to reduce the original N_v visual tokens to n_v critical tokens. DOP directly integrates with different visual token reduction methods. In this work, we mainly adopt two token pruning methods: VisPruner (Zhang et al., 2024a) based on [CLS] attention and similarity, and CDPruner (Zhang et al., 2025) based on conditional diversity, along with visual input resizing for Qwen2.5-VL (Bai et al., 2025) and InternVL3 (Zhu et al., 2025).

Layer Positions and Module Types. We use layer position l and module type m to identify specific MHA/MLP operations. The layer position $l \in \{1, \dots, L\}$ where L is the number of decoder layers. Within each layer, we focus on two modules consuming most computation within a layer: *MHA* for mutual token feature updating, and *MLP* for independent token-wise feature transformation.

Policy Space Size. While our fine-grained operation pruning paradigm enables more precise computation control, it exponentially expands the policy space. For a 32-layer decoder with $|\mathcal{M}| = 2$ module types and $N_v = 576$ visual tokens, there are $|\mathcal{O}_v| = 32 \times 2 = 64$ visual operations. With binary decisions for each operation and 577 possible token counts (0 to 576), the total pruning configurations become: $2^{64} \times 577 \approx 1.0 \times 10^{22}$. Such an enormous policy space necessitates efficient optimization to avoid prohibitive computational costs.

3.2 PRUNING POLICY OPTIMIZATION

In this section, we introduce DOP’s policy optimization for pruning visual operations based on depth-wise pruning and additive approximation, as shown in Figures 2b and 2c. Note that we focus on visual token operations since they are most numerous and constitute the majority of computational overhead, while also enabling fair comparison with baselines that only prune visual tokens.

3.2.1 DEPTH-WISE OPERATION PRUNING

Deeper layers are typically more redundant in LLMs (Gromov et al.). While deeper operations are not necessarily more redundant than shallower ones across different module types or token groups, we observe that for the same group-module type (g, m) , a deeper operation (g, l_2, m) remains generally more redundant than a shallower operation (g, l_1, m) with $l_2 > l_1$.

Depth-wise Pruning Constraint. For each module type $m \in \{MHA, MLP\}$ and token group g , operations are pruned consecutively from the deepest layer. Operation (g, l, m) being pruned implies that operations $(g, l + 1, m), \dots, (g, L, m)$ are also pruned.

Depth-wise Pruning Policy. When applying depth-wise pruning only for visual token group \mathbf{g}_v operations, a pruning policy can be parameterized by 3 parameters:

$$(d_A, d_P, n_v), \text{ where } d_A, d_P \in \{0, \dots, L\}, n_v \in \{0, \dots, N_v\}, \quad (3)$$

representing MHA depth, MLP depth, and the number of visual tokens, respectively. Here, L is the total number of layers and N_v is the original visual token count. As shown in Figure 2b, all MHA operations $\{(\mathbf{g}_v, l, MHA)\}_{l=d_A+1}^L$ beyond layer d_A and all MLP operations $\{(\mathbf{g}_v, l, MLP)\}_{l=d_P+1}^L$ beyond layer d_P are pruned:

$$\mathcal{P}(d_A, d_P) = \{(\mathbf{g}_v, l, MHA)\}_{l=d_A+1}^L \cup \{(\mathbf{g}_v, l, MLP)\}_{l=d_P+1}^L. \quad (4)$$

The remaining visual operations $\{(\mathbf{g}_v, l, MHA)\}_{l=1}^{d_A} \cup \{(\mathbf{g}_v, l, MLP)\}_{l=1}^{d_P}$ process only n_v visual tokens in \mathbf{g}_v that are retained after token reduction.

In effect, this policy creates a “visual processing cutoff” where visual tokens are first reduced to n_v before decoder, then processed through shallow MHA and MLP modules up to depths d_A and d_P respectively, while deeper MHA and MLP modules operate without any visual information.

Policy Space Size. For a 32-layer decoder with $|\mathcal{M}| = 2$ and $N_v = 576$, depth-wise pruning reduces possible pruning policies from 1.0×10^{22} to $(|\mathcal{L}| + 1)^{|\mathcal{M}|} \times (N_v + 1) = 33^2 \times 577 = 628, 353$. However, this remains huge, motivating further optimization complexity reduction.

3.2.2 POLICY OPTIMIZATION WITH ADDITIVE APPROXIMATION

The optimization of the three DOP policy parameters constitutes a combinatorial optimization problem where a naive approach is to exhaustively evaluate all possible policies, formulated as follows:

$$(d_A^*, d_P^*, n_v^*) = \arg \min_{\substack{d_A, d_P \in \{0, 1, \dots, L\} \\ n_v \in \{0, 1, \dots, N_v\}}} \mathcal{D}(d_A, d_P, n_v) \quad \text{s.t.} \quad \text{TFLOPs}(d_A, d_P, n_v) \leq \tau, \quad (5)$$

where L is the total number of decoder layers and N_v is the original visual token count. We minimize $\mathcal{D}(d_A, d_P, n_v)$, the divergence from the original model’s output distribution caused by pruning policy (d_A, d_P, n_v) , as greater deviation typically indicates worse performance, and divergence can be computed without labels, reducing data leakage concerns. Theoretical FLOPs (TFLOPs) is used to measure computational cost after pruning with budget τ . We detail the computation of divergence and TFLOPs in Sections C.2 and C.3 respectively.

To solve Equation (5), we must evaluate $\mathcal{D}(d_A, d_P, n_v)$ for all possible policies with $(L+1)^2 \times (N_v+1) + 1$ model runs over the validation set, while subsequent TFLOPs computation, exhaustive search through recorded divergences, and comparisons can be completed with negligible cost. Therefore, we reduce optimization cost by minimizing the required validation runs.

Additive Approximation. We apply an additive approximation by replacing the joint divergence $\mathcal{D}(d_A, d_P, n_v)$ in Equation (5) with the sum of individual divergences:

$$\mathcal{D}_{\text{sum}}(d_A, d_P, n_v) = \mathcal{D}_A(d_A) + \mathcal{D}_P(d_P) + \mathcal{D}_v(n_v) = \mathcal{D}(d_A, L, N_v) + \mathcal{D}(L, d_P, N_v) + \mathcal{D}(L, L, n_v).$$

We only need $L + 1$, $L + 1$, and $N_v + 1$ model runs for $\mathcal{D}_A(d_A)$, $\mathcal{D}_P(d_P)$, and $\mathcal{D}_v(n_v)$ respectively, resulting in $2L + N_v + 4$ validation runs including one for the original model.

Since solving Equation (5) does not require exact $\mathcal{D}(d_A, d_P, n_v)$ values but only relative policy rankings based on it, the key to yielding good policies when using \mathcal{D}_{sum} to replace \mathcal{D} is ensuring that \mathcal{D}_{sum} results in largely consistent policy rankings with \mathcal{D} such that the following largely holds:

$$\mathcal{D}_{\text{sum}}(d_A, d_P, n_v) > \mathcal{D}_{\text{sum}}(d'_A, d'_P, n'_v) \Rightarrow \mathcal{D}(d_A, d_P, n_v) > \mathcal{D}(d'_A, d'_P, n'_v), \quad (6)$$

which is validated by sampling policies, computing both \mathcal{D} and \mathcal{D}_{sum} , and calculating Spearman’s rank correlation between their rankings in Section E.1. Results show strong positive correlations across models ($\rho \geq 0.799$, $p < 10^{-48}$), supporting our additive approximation.

Final Policy Optimization. Besides additive approximation, we employ sparse sampling for divergence evaluation with interpolation (Section C.1) and add visual token count constraints to avoid overly conservative operation pruning (Section C.4), yielding the final optimization:

$$\begin{aligned} (d_A^*, d_P^*, n_v^*) = \arg \min_{(d_A, d_P, n_v)} & \hat{\mathcal{D}}_A(d_A) + \hat{\mathcal{D}}_P(d_P) + \hat{\mathcal{D}}_v(n_v) \\ \text{s.t.} & \text{TFLOPs}(d_A, d_P, n_v) \leq \tau \\ & n_v \geq n_{\min} \end{aligned} \quad (7)$$

where $\hat{\mathcal{D}}_A$, $\hat{\mathcal{D}}_P$, $\hat{\mathcal{D}}_v$ are interpolated individual divergences for MHA depth, MLP depth, and visual token count respectively and n_{\min} is the minimum visual token count.

With I sampling points per parameter, we need only $3 \cdot I + 1$ validation runs as a one-time cost. Once completed, optimizing policies for different constraints only requires solving Equation (7) by enumerating policies, computing TFLOPs, and comparing the sum of recorded individual divergences for policies that satisfy the constraints with negligible cost compared to validation runs.

4 EXPERIMENTS

In this section, we evaluate DOP on 6 MLLM models and 13 multimodal benchmarks against 12 baselines, report real GPU acceleration and optimization costs, demonstrate flexibility with three token reduction methods, and conduct extensive ablations on cross-task and cross-architecture generalization as well as optimization data-efficiency.

4.1 EXPERIMENTAL SETUP

MLLM Models. We apply DOP to 6 MLLM models, including LLaVA-1.5 (7B & 13B) (Liu et al., 2024b) and LLaVA-Next (7B & 13B) (Liu et al., 2024a), Qwen2.5-VL (7B) (Bai et al., 2025) and InternVL3-8B (Zhu et al., 2025). Model details are in Section D.1.

Evaluation Benchmarks. We select 13 benchmarks for evaluation, including 9 general VQA tasks: VQA^{V2} (Goyal et al., 2017), VizWiz (Gurari et al., 2018), ScienceQA (SQA^I) (Saikh et al., 2022), GQA (Hudson & Manning, 2019), SeedBench (Seed^I) (Li et al., 2023a), MME (Fu et al., 2023), POPE (Li et al., 2023c), MMBench (MMB), MMBench-CN (MMB^{CN}) (Liu et al., 2023b); and 4 text-oriented VQA tasks: TextVQA (VQA^{text}) (Singh et al., 2019) AI2D (Kembhavi et al., 2016) ChartQA (Masry et al., 2022), and OCRBench (Liu et al., 2024c). Details are in Section D.2.

Baselines. We compare DOP with 12 baselines, including FastV (Chen et al., 2024), FitPrune (Ye et al., 2024), PyramidDrop (PDrop) (Xing et al., 2024), SparseVLM (Zhang et al., 2024c), PruMerge (Shang et al., 2024), VisionZip (Yang et al., 2024), TRIM (Song et al., 2025), DART (Wen

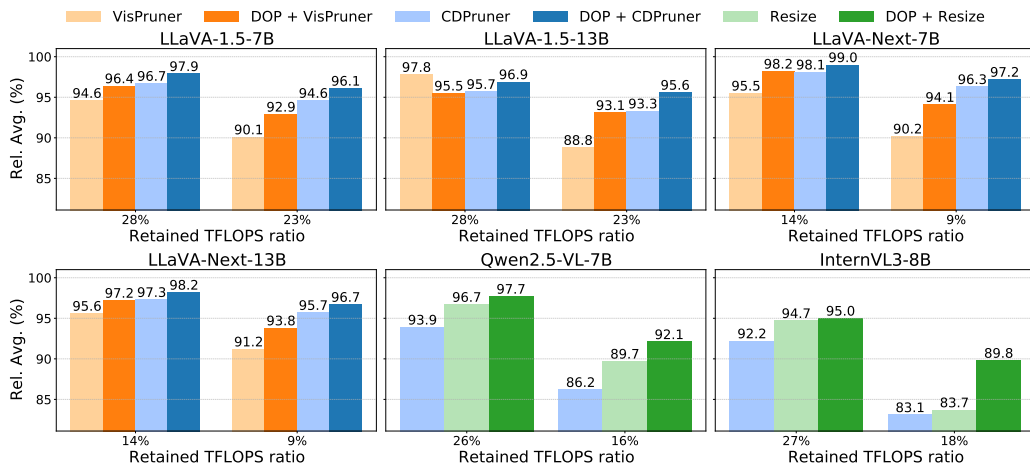


Figure 3: Overview of DOP performance across LLaVA-1.5-7B&13B (Liu et al., 2024b), LLaVA-Next-7B&13B (Liu et al., 2024a), Qwen2.5-VL-7B (Bai et al., 2025) and InternVL3-8B (Zhu et al., 2025). Rel. Avg. is the mean performance ratio relative to the original model, averaged across benchmarks used for each model. DOP is flexible with various token reduction methods and consistently boosts the performance of corresponding baselines.

Method	VQA ^{v2}	GQA	VizWiz	SQA ^I	Seed ^I	VQA ^{Text}	POPE	MME	MMB	MMB ^{CN}	Rel. Avg.
<i>Upper Bound: 100% TFLOPs (= 576 Visual Tokens Every Layer)</i>											
LLaVA-1.5-7B	78.5	61.9	50.1	69.5	66.2	58.2	85.9	1506.5	64.7	58.1	100%
<i>Retain 28% TFLOPs (= 64 Visual Tokens Every Layer)</i>											
FastV (Chen et al., 2024)	55.9	46.0	49.1	70.1	51.9	51.6	35.5	973.5	50.1	42.1	76.7%
FitPrune (Ye et al., 2024)	63.7	52.3	51.1	68.0	55.8	51.2	73.6	1287.5	58.5	49.7	88.5%
DivPrune (Alvar et al., 2025)	74.1	57.5	53.6	68.0	61.7	54.5	85.5	1334.7	60.1	52.3	95.0%
VisPruner (Zhang et al., 2024a)	72.7	55.4	53.3	69.1	58.5	55.8	80.4	1369.9	61.3	55.1	94.6%
DOP_V (Ours)	74.6	57.1	53.6	69.2	60.3	56.5	83.1	1394.6	61.6	56.5	96.4%
CDPruner (Zhang et al., 2025)	75.4	58.6	53.4	68.1	62.5	55.3	87.5	1415.1	61.1	53.2	96.7%
DOP_{CD} (Ours)	76.2	59.6	53.4	68.3	63.6	55.8	87.6	1436.3	62.4	55.1	97.9%
<i>Retain 23% TFLOPs (= 32 Visual Tokens Every Layer)</i>											
DivPrune (Alvar et al., 2025)	71.2	54.9	53.3	68.6	58.7	52.9	81.5	1284.9	57.6	49.1	91.8%
VisPruner (Zhang et al., 2024a)	67.7	52.2	53.0	69.2	54.3	53.9	72.7	1271.0	58.4	52.7	90.1%
DOP_V (Ours)	71.0	54.8	53.9	69.1	56.7	54.5	79.6	1306.5	59.4	53.7	92.9%
CDPruner (Zhang et al., 2025)	73.6	57.0	53.1	69.5	60.9	53.2	87.9	1373.0	59.6	49.6	94.6%
DOP_{CD} (Ours)	74.7	58.1	53.6	69.3	62.2	54.2	87.9	1397.5	60.1	52.2	96.1%

Table 1: **Performance comparison on LLaVA-1.5-7B (Liu et al., 2024b)**. Rel. Avg. is the mean performance ratio relative to the original model averaged across all benchmarks. **Bold** indicates the best at each TFLOPs ratio. DOP_V uses VisPruner to reduce visual tokens, while DOP_{CD} uses CDPruner. Our comparison matches actual TFLOPs and notes the per-layer token counts that achieve these TFLOPs. See Tables 8 and 9 for full comparison across LLaVA-1.5-7B&13B.

et al., 2025), DivPrune (Alvar et al., 2025), VisPruner (Zhang et al., 2024a) and CDPruner (Zhang et al., 2025). PDrop, FitPrune, and SparseVLM are progressive pruning methods, with FitPrune using the same validation set for pruning policy optimization. Details are in Section D.3.

DOP Configurations. DOP only prunes visual token operations, sampling $K = 6$ points for visual token count, MHA depth, and MLP depth respectively to evaluate output divergence on 100 randomly selected TextVQA training samples for each model. Each model applies the same optimized policy across all benchmarks at each TFLOPs ratio. For LLaVA, we evaluate DOP_V and DOP_{CD} with VisPruner and CDPruner for visual token reduction, while for Qwen2.5-VL and InternVL3, we evaluate DOP_R with input image resizing. Additional configuration details are in Section D.4.

Method	VQA ^{v2}	GQA	VizWiz	SQA ¹	Seed ¹	VQA ^{Text}	POPE	MME	MMB	MMB ^{CN}	Rel. Avg.
<i>Upper Bound: 100% TFLOPs (= 2880 Visual Tokens Every Layer)</i>											
LLaVA-NeXT-7B	81.3	62.5	55.2	67.5	70.2	60.3	86.8	1511.8	65.8	57.3	100.0%
<i>Retain 14% TFLOPs (= 320 Visual Tokens Every Layer)</i>											
FastV Chen et al. (2024)	61.5	49.8	51.3	66.6	58.6	52.2	49.5	1099.0	53.4	42.5	80.2%
DivPrune Alvar et al. (2025)	77.2	61.1	55.6	67.7	67.1	56.2	84.7	1423.3	63.9	55.7	96.9%
VisPruner	75.7	58.4	57.0	69.5	62.8	57.6	80.4	1370.1	63.6	55.8	95.5%
DOP_V (Ours)	77.6	60.4	56.4	69.7	65.2	59.2	84.6	1455.7	65.1	57.5	98.2%
CDPruner Zhang et al. (2025)	78.4	61.6	55.8	67.8	67.3	57.4	87.2	1453.0	65.5	55.7	98.1%
DOP_{CD} (Ours)	79.1	61.7	55.4	68.0	68.4	57.9	87.4	1472.9	66.8	56.9	99.0%
<i>Retain 9% TFLOPs (= 160 Visual Tokens Every Layer)</i>											
DivPrune Alvar et al. (2025)	75.0	59.3	56.1	67.1	64.9	54.1	80.0	1356.6	62.9	53.7	94.2%
VisPruner	70.6	54.7	57.1	68.6	58.1	56.0	72.7	1226.0	60.5	51.4	90.2%
DOP_V (Ours)	74.1	57.6	56.5	68.7	61.2	57.1	79.4	1355.6	62.1	55.1	94.1%
CDPruner Zhang et al. (2025)	76.7	60.8	55.2	67.5	65.9	55.4	86.8	1425.3	64.2	53.8	96.3%
DOP_{CD} (Ours)	77.5	61.2	55.1	67.5	66.7	56.7	87.5	1446.4	64.8	55.1	97.2%

Table 2: **Performance comparison on LLaVA-NeXT-7B (Liu et al., 2024a)**. Rel. Avg. is the mean performance ratio relative to the original model averaged across all benchmarks. **Bold** indicates the best at each TFLOPs ratio. DOP_V uses VisPruner to reduce visual tokens, while DOP_{CD} uses CDPruner. Our comparison matches TFLOPs and notes the per-layer token counts needed to achieve these budgets. Full comparison across LLaVA-Next-7B&13B are in Tables 10 and 11.

Model	TFLOPs	Method	Prefilling (ms)			Sample (ms)			Total Time (min)			Cost (min)
			EA	SA	FA	EA	SA	FA	EA	SA	FA	
LLaVA-1.5-7B	100%	-	73	59	60	133	118	122	27	25	26	-
	28%	CDPruner	28	26	26	93	86	85	13	12	12	-
		DOP _{CD}	28	26	26	93	86	87	13	12	13	5
LLaVA-Next-7B	100%	-	494	253	254	593	346	350	64	43	44	-
	14%	CDPruner	52	45	45	141	127	127	17	16	16	-
		DOP _{CD}	53	44	44	143	128	127	17	16	16	12

Table 3: **Efficiency and Cost on NVIDIA A100-80G GPU**. We report the average prefiling and sample latencies as well as total response time over 5000 TextVQA samples for LLaVA-1.5-7B and LLaVA-Next-7B using three attention implementations: Eager (EA), SDPA (SA), and FlashAttention2 (Dao et al., 2022) (FA). We also report the one-time cost for evaluating sampled individual divergences on 100 TextVQA samples with eager attention, where other costs for optimizing DOP are negligible. We only report DOP_{CD} as DOP_V has identical efficiency and cost.

4.2 RESULTS AND COMPARISONS

Overall Performance. Figure 3 shows DOP’s performance across all selected models. DOP consistently improves different token reduction methods and outperforms state-of-the-art baseline CDPruner by up to 7%. The advantages of DOP become more pronounced at lower TFLOPs ratios, demonstrating that tighter computational budgets require more precise and fine-grained control over computation, validating DOP’s improvement direction. All policies are in Tables 15 and 16

LLaVA-series Models. Tables 1 and 2 present selected evaluation results on LLaVA-1.5-7B (Liu et al., 2024b) and LLaVA-Next-7B (Liu et al., 2024a), with full comparison across LLaVA-1.5-7B&13B and LLaVA-Next-7B&13B in Tables 8 to 11. We evaluate DOP_V and DOP_{CD} with VisPruner and CDPruner for visual token reduction respectively. DOP consistently outperforms all baselines, demonstrating superior performance-efficiency tradeoffs and flexibility across visual token reduction methods. TextVQA-optimized policies generalize well across tasks. Notably, while progressive pruning methods (FitPrune, PDrop, SparseVLM) performance rapidly degrades at lower TFLOPs ratios, DOP’s improvements become more pronounced, validating the benefits of refining token allocation granularity from layer-level to module-level.

Qwen2.5-VL and InternVL3. Tables 12 and 13 evaluate DOP_R with input image resizing on Qwen2.5-VL-7B (Bai et al., 2025) and InternVL3-8B (Zhu et al., 2025). We include text-oriented VQA benchmarks (TextVQA, ChartQA, AI2D, OCRBench) that are more sensitive to visual information. DOP consistently improves performance across all settings, with notable improvements up to 24% on text-oriented benchmarks, demonstrating that DOP preserves more critical visual

Validation	Evaluation Set										Rel. Avg.
	VQA ^{v2}	GQA	VizWiz	SQA ¹	Seed ¹	VQA ^{Text}	POPE	MME	MMB	MMB ^{CN}	
VQA ^{Text}	76.2	59.6	53.4	68.3	63.6	55.8	87.6	1436.3	62.4	55.1	97.9%
Seed ¹	60.5	50.3	45.9	67.6	64.2	50.5	85.0	1442.4	62.7	55.3	91.8%
VQA ^{v2}	76.0	59.5	53.3	68.3	63.5	55.8	87.6	1408.6	61.7	54.1	97.3%

Table 4: **Cross-task Generalization Ablation** with optimizing DOP_{CD} for LLaVA-1.5-7B at 28% TFLOPs with 100 samples from TextVQA, SeedBench, and VQAv2. TextVQA and VQAv2 policies generalize well across tasks, while SeedBench policies show poor generalization.

Model	LLaVA-1.5	LLaVA-Next	Qwen2.5-VL	InternVL3
Size	13B	7B / 13B	7B	8B
TFLOPs	28%	14% / 14%	26%	27%
Direct	96.9%	99.0% / 98.2%	97.7%	95.0%
Transfer	96.7%	98.8% / 98.2%	97.4%	94.3%

Table 5: **Cross-Model Generalization Ablation**. Direct denotes DOP optimized directly on the target model, while Transfer denotes DOP with divergences transferred from DOP on LLaVA-1.5-7B (detailed in Section C.5). We use DOP_{CD} for LLaVA and DOP_R for Qwen2.5-VL and InternVL3. Results are the relative average performance (**Rel. Avg.**) compared to each original model.

details than uniform allocation. Additionally, while CDPruner and DivPrune struggle on these non-LLaVA models against basic FastV and resizing baselines—contrasting with their advantages on LLaVA—this raises concerns about overfitting to model-specific patterns. In contrast, DOP maintains consistent gains across architectures, indicating that fine-grained token allocation effectively improves performance-efficiency tradeoffs across different architectures.

Efficiency and Cost on Real GPU. Table 3 reports efficiency gains and optimization costs on a single NVIDIA A100-80G GPU for LLaVA-1.5-7B and LLaVA-Next-7B, with the costs for other models shown in Table 17. DOP’s TFLOPs reduction translates well to real device efficiency, with particularly notable improvements in prefilling stage latency, which is our target. We tested three commonly used attention implementations and found DOP directly compatible with all. Compared to CDPruner under the same computational budget, DOP achieves comparable acceleration. Our optimization is also highly efficient with costs under 18 minutes for all models (Table 14), further reducible to 2 minutes using 25 samples (Section F.1), confirming deployment feasibility.

5 ABLATION STUDY

In this section, we conduct ablation studies on cross-task and cross-model generalization capabilities. Additional ablations are in Section F.

Cross-task Generalization. Table 4 evaluates DOP’s cross-task generalization by optimizing policies on VQAv2 and SeedBench with 100 samples each, and shows a clear ranking: TextVQA policy \geq VQAv2 policy \gg SeedBench policy. According to Section F.2, this stems from different redundancy distributions across task types. SeedBench exhibits significantly greater deep-layer redundancy due to its multiple-choice format requiring only shallow visual processing, leading to aggressive deep pruning that fails to generalize to tasks requiring deep operations. Conversely, policies from tasks requiring deep operations generalize well to tasks like SeedBench, validating our TextVQA optimization choice.

Cross-model Generalization. Table 5 shows the results of generalizing DOP_{CD} on LLaVA-1.5-7B to other models by transferring the individual divergences according to Section C.5. Results show that transferred DOP achieves comparable performance to direct optimization on target models, with differences within 0.7%. This indicates similar redundancy distributions across MLLMs, enabling strong cross-model generalization and reducing deployment costs by optimizing once and transferring to all models. Additionally, transferring DOP_{CD} divergences to DOP_R for Qwen2.5-VL and InternVL3 demonstrates effective generalization across different token reduction methods.

6 CONCLUSION

In this work, we investigated computational redundancy in MLLMs and addressed the limitation of prior token reduction that overlooks structural redundancy by proposing DOP, an operation pruning method that enables adjusting different modules’ token loads based on their redundancy levels. DOP ensures efficient optimization through depth-wise pruning constraints and additive approximation techniques. Our comprehensive evaluation demonstrates that DOP preserves up to 7% more performance than state-of-the-art token reduction methods across 6 MLLM models and 13 tasks, with TFLOPs reductions translating effectively to acceleration on real GPUs. Ablation studies further reveal DOP’s optimization efficiency and strong generalization capabilities, confirming its practical value for deploying MLLMs in resource-constrained environments.

7 REPRODUCIBILITY STATEMENT

We will release our complete code implementation upon acceptance to ensure full reproducibility of our results. Detailed method configurations and implementation specifics are provided in Section D and all the optimized DOP policies are in Tables 15 and 16. Our released codebase will include functionality for optimizing and evaluating DOP policies across all models and benchmarks utilized in this work, facilitating straightforward extension to additional models and benchmarks as well as seamless comparison with other methods.

8 ETHICS STATEMENT

DOP is designed to improve MLLM efficiency while preserving performance. This is a general technical improvement without any purpose or direct applications we can anticipate that would raise ethical considerations. We encourage responsible use of DOP and recommend that users avoid deploying it for applications that may raise ethical considerations.

REFERENCES

- Marah Abdin, Jyoti Aneja, Hany Awadalla, Ahmed Awadallah, Ammar Ahmad Awan, Nguyen Bach, Amit Bahree, Arash Bakhtiari, Jianmin Bao, Harkirat Behl, et al. Phi-3 technical report: A highly capable language model locally on your phone. *arXiv preprint arXiv:2404.14219*, 2024.
- Josh Achiam, Steven Adler, Sandhini Agarwal, Lama Ahmad, Ilge Akkaya, Florencia Leoni Aleman, Diogo Almeida, Janko Altenschmidt, Sam Altman, Shyamal Anadkat, et al. Gpt-4 technical report. *arXiv:2303.08774*, 2023.
- Harsh Agrawal, Karan Desai, Yufei Wang, Xinlei Chen, Rishabh Jain, Mark Johnson, Dhruv Batra, Devi Parikh, Stefan Lee, and Peter Anderson. Nocaps: Novel object captioning at scale. In *Proceedings of the IEEE/CVF international conference on computer vision*, pp. 8948–8957, 2019.
- Saeed Ranjbar Alvar, Gursimran Singh, Mohammad Akbari, and Yong Zhang. Divprune: Diversity-based visual token pruning for large multimodal models. In *Proceedings of the Computer Vision and Pattern Recognition Conference*, pp. 9392–9401, 2025.
- Jinze Bai, Shuai Bai, Yunfei Chu, Zeyu Cui, Kai Dang, Xiaodong Deng, Yang Fan, Wenbin Ge, Yu Han, Fei Huang, et al. Qwen technical report. *arXiv:2309.16609*, 2023a.
- Jinze Bai, Shuai Bai, Shusheng Yang, Shijie Wang, Sinan Tan, Peng Wang, Junyang Lin, Chang Zhou, and Jingren Zhou. Qwen-VL: A frontier large vision-language model with versatile abilities. *arXiv:2308.12966*, 2023b.
- Shuai Bai, Keqin Chen, Xuejing Liu, Jialin Wang, Wenbin Ge, Sibao Song, Kai Dang, Peng Wang, Shijie Wang, Jun Tang, Humen Zhong, Yuanzhi Zhu, Mingkun Yang, Zhaohai Li, Jianqiang Wan, Pengfei Wang, Wei Ding, Zheren Fu, Yiheng Xu, Jiabo Ye, Xi Zhang, Tianbao Xie, Zesen Cheng, Hang Zhang, Zhibo Yang, Haiyang Xu, and Junyang Lin. Qwen2.5-vl technical report. *arXiv preprint arXiv:2502.13923*, 2025.

-
- Tom Brown, Benjamin Mann, Nick Ryder, Melanie Subbiah, Jared D Kaplan, Prafulla Dhariwal, Arvind Neelakantan, Pranav Shyam, Girish Sastry, Amanda Askell, et al. Language models are few-shot learners. *Advances in neural information processing systems*, 2020.
- Liang Chen, Haozhe Zhao, Tianyu Liu, Shuai Bai, Junyang Lin, Chang Zhou, and Baobao Chang. An image is worth 1/2 tokens after layer 2: Plug-and-play inference acceleration for large vision-language models. In *Proceedings of the European Conference on Computer Vision (ECCV)*, 2024.
- Lin Chen, Jisong Li, Xiaoyi Dong, Pan Zhang, Conghui He, Jiaqi Wang, Feng Zhao, and Dahua Lin. Sharegpt4v: Improving large multi-modal models with better captions. *arXiv:2311.12793*, 2023a.
- Xinlei Chen, Hao Fang, Tsung-Yi Lin, Ramakrishna Vedantam, Saurabh Gupta, Piotr Dollár, and C Lawrence Zitnick. Microsoft coco captions: Data collection and evaluation server. *arXiv preprint arXiv:1504.00325*, 2015.
- Zhe Chen, Jiannan Wu, Wenhai Wang, Weijie Su, Guo Chen, Sen Xing, Muyan Zhong, Qinglong Zhang, Xizhou Zhu, Lewei Lu, Bin Li, Ping Luo, Tong Lu, Yu Qiao, and Jifeng Dai. InternVL: Scaling up vision foundation models and aligning for generic visual-linguistic tasks. *arXiv:2312.14238*, 2023b.
- Wenliang Dai, Junnan Li, Dongxu Li, Anthony Tiong, Junqi Zhao, Weisheng Wang, Boyang Li, Pascale Fung, and Steven Hoi. InstructBLIP: Towards general-purpose vision-language models with instruction tuning. *Advances in Neural Information Processing Systems*, 2023.
- Tri Dao, Dan Fu, Stefano Ermon, Atri Rudra, and Christopher Ré. Flashattention: Fast and memory-efficient exact attention with io-awareness. *Advances in Neural Information Processing Systems*, 35:16344–16359, 2022.
- Zhengxiao Du, Yujie Qian, Xiao Liu, Ming Ding, Jiezhong Qiu, Zhilin Yang, and Jie Tang. GLM: General language model pretraining with autoregressive blank infilling. *arXiv:2103.10360*, 2021.
- Chaoyou Fu, Peixian Chen, Yunhang Shen, Yulei Qin, Mengdan Zhang, Xu Lin, Jinrui Yang, Xiawu Zheng, Ke Li, Xing Sun, et al. MME: A comprehensive evaluation benchmark for multimodal large language models. *arXiv:2306.13394*, 2023.
- Yash Goyal, Tejas Khot, Douglas Summers-Stay, Dhruv Batra, and Devi Parikh. Making the v in vqa matter: Elevating the role of image understanding in visual question answering. In *Proceedings of the IEEE conference on computer vision and pattern recognition*, pp. 6904–6913, 2017.
- Andrey Gromov, Kushal Tirumala, Hassan Shapourian, Paolo Glorioso, and Dan Roberts. The unreasonable ineffectiveness of the deeper layers. In *The Thirteenth International Conference on Learning Representations*.
- Suriya Gunasekar, Yi Zhang, Jyoti Aneja, Caio César Teodoro Mendes, Allie Del Giorno, Sivakanth Gopi, Mojan Javaheripi, Piero Kauffmann, Gustavo de Rosa, Olli Saarikivi, et al. Textbooks are all you need. *arXiv preprint arXiv:2306.11644*, 2023.
- Danna Gurari, Qing Li, Abigale J Stangl, Anhong Guo, Chi Lin, Kristen Grauman, Jiebo Luo, and Jeffrey P Bigham. Vizwiz grand challenge: Answering visual questions from blind people. In *Proceedings of the IEEE conference on computer vision and pattern recognition*, pp. 3608–3617, 2018.
- Drew A Hudson and Christopher D Manning. GQA: A new dataset for real-world visual reasoning and compositional question answering. *Conference on Computer Vision and Pattern Recognition (CVPR)*, 2019.
- Aniruddha Kembhavi, Mike Salvato, Eric Kolve, Minjoon Seo, Hannaneh Hajishirzi, and Ali Farhadi. A diagram is worth a dozen images. In *European conference on computer vision*, pp. 235–251. Springer, 2016.

-
- Ivan Krasin, Tom Duerig, Neil Alldrin, Vittorio Ferrari, Sami Abu-El-Haija, Alina Kuznetsova, Hassan Rom, Jasper Uijlings, Stefan Popov, Andreas Veit, et al. Openimages: A public dataset for large-scale multi-label and multi-class image classification. *Dataset available from <https://github.com/openimages>*, 2(3):18, 2017.
- Ranjay Krishna, Yuke Zhu, Oliver Groth, Justin Johnson, Kenji Hata, Joshua Kravitz, Stephanie Chen, Yannis Kalantidis, Li-Jia Li, David A Shamma, et al. Visual genome: Connecting language and vision using crowdsourced dense image annotations. *International journal of computer vision*, 123(1):32–73, 2017.
- Woosuk Kwon, Zhuohan Li, Siyuan Zhuang, Ying Sheng, Lianmin Zheng, Cody Hao Yu, Joseph Gonzalez, Hao Zhang, and Ion Stoica. Efficient memory management for large language model serving with pagedattention. In *Proceedings of the 29th Symposium on Operating Systems Principles*, pp. 611–626, 2023.
- Bohao Li, Rui Wang, Guangzhi Wang, Yuying Ge, Yixiao Ge, and Ying Shan. Seed-bench: Benchmarking multimodal llms with generative comprehension. *arXiv:2307.16125*, 2023a.
- Junnan Li, Dongxu Li, Silvio Savarese, and Steven Hoi. Blip-2: Bootstrapping language-image pre-training with frozen image encoders and large language models. In *International conference on machine learning*, 2023b.
- Yanwei Li, Chengyao Wang, and Jiaya Jia. LLaMA-VID: An image is worth 2 tokens in large language models. In *Proceedings of the IEEE/CVF Conference on Computer Vision and Pattern Recognition*, 2024.
- Yifan Li, Yifan Du, Kun Zhou, Jinpeng Wang, Wayne Xin Zhao, and Ji-Rong Wen. Evaluating object hallucination in large vision-language models. *arXiv:2305.10355*, 2023c.
- Bin Lin, Bin Zhu, Yang Ye, Munan Ning, Peng Jin, and Li Yuan. Video-llava: Learning united visual representation by alignment before projection. *arXiv:2311.10122*, 2023a.
- Ji Lin, Hongxu Yin, Wei Ping, Yao Lu, Pavlo Molchanov, Andrew Tao, Huizi Mao, Jan Kautz, Mohammad Shoeybi, and Song Han. Vila: On pre-training for visual language models, 2023b.
- Zhihang Lin, Mingbao Lin, Luxi Lin, and Rongrong Ji. Boosting multimodal large language models with visual tokens withdrawal for rapid inference. *arXiv preprint arXiv:2405.05803*, 2024.
- Aoming Liu, Zehao Huang, Zhiwu Huang, and Naiyan Wang. Direct differentiable augmentation search. In *Proceedings of the IEEE/CVF international conference on computer vision*, pp. 12219–12228, 2021.
- Hanxiao Liu, Karen Simonyan, and Yiming Yang. Darts: Differentiable architecture search. *arXiv preprint arXiv:1806.09055*, 2018.
- Haotian Liu, Chunyuan Li, Yuheng Li, and Yong Jae Lee. Improved baselines with visual instruction tuning. *arXiv:2310.03744*, 2023a.
- Haotian Liu, Chunyuan Li, Yuheng Li, Bo Li, Yuanhan Zhang, Sheng Shen, and Yong Jae Lee. Llava-next: Improved reasoning, ocr, and world knowledge, January 2024a. URL <https://llava-vl.github.io/blog/2024-01-30-llava-next/>.
- Haotian Liu, Chunyuan Li, Qingyang Wu, and Yong Jae Lee. Visual instruction tuning. *Advances in neural information processing systems*, 2024b.
- Yuan Liu, Haodong Duan, Yuanhan Zhang, Bo Li, Songyang Zhang, Wangbo Zhao, Yike Yuan, Jiaqi Wang, Conghui He, Ziwei Liu, et al. MMBench: Is your multi-modal model an all-around player? *arXiv:2307.06281*, 2023b.
- Yuliang Liu, Zhang Li, Mingxin Huang, Biao Yang, Wenwen Yu, Chunyuan Li, Xu-Cheng Yin, Cheng-Lin Liu, Lianwen Jin, and Xiang Bai. Ocrbench: on the hidden mystery of ocr in large multimodal models. *Science China Information Sciences*, 67(12), December 2024c. ISSN 1869-1919. doi: 10.1007/s11432-024-4235-6. URL <http://dx.doi.org/10.1007/s11432-024-4235-6>.

-
- Pan Lu, Swaroop Mishra, Tanglin Xia, Liang Qiu, Kai-Wei Chang, Song-Chun Zhu, Oyvind Tafjord, Peter Clark, and Ashwin Kalyan. Learn to explain: Multimodal reasoning via thought chains for science question answering. *Advances in Neural Information Processing Systems*, 35:2507–2521, 2022.
- Ahmed Masry, Do Xuan Long, Jia Qing Tan, Shafiq Joty, and Enamul Hoque. Chartqa: A benchmark for question answering about charts with visual and logical reasoning. *arXiv preprint arXiv:2203.10244*, 2022.
- Baolin Peng, Chunyuan Li, Pengcheng He, Michel Galley, and Jianfeng Gao. Instruction tuning with gpt-4. *arXiv:2304.03277*, 2023.
- Bryan A Plummer, Liwei Wang, Chris M Cervantes, Juan C Caicedo, Julia Hockenmaier, and Svetlana Lazebnik. Flickr30k entities: Collecting region-to-phrase correspondences for richer image-to-sentence models. In *Proceedings of the IEEE international conference on computer vision*, pp. 2641–2649, 2015.
- Alec Radford, Jong Wook Kim, Chris Hallacy, Aditya Ramesh, Gabriel Goh, Sandhini Agarwal, Girish Sastry, Amanda Askell, Pamela Mishkin, Jack Clark, et al. Learning transferable visual models from natural language supervision. In *International conference on machine learning*, pp. 8748–8763. PMLR, 2021.
- Tanik Saikh, Tirthankar Ghosal, Amish Mittal, Asif Ekbal, and Pushpak Bhattacharyya. Scienceqa: A novel resource for question answering on scholarly articles. *International Journal on Digital Libraries*, 23(3):289–301, 2022.
- Anthony Sarah, Sharath Nittur Sridhar, Maciej Szankin, and Sairam Sundaresan. Llama-nas: Efficient neural architecture search for large language models. In *European Conference on Computer Vision*, pp. 67–74. Springer, 2025.
- Yuzhang Shang, Mu Cai, Bingxin Xu, Yong Jae Lee, and Yan Yan. Llava-prumerge: Adaptive token reduction for efficient large multimodal models. *arXiv preprint arXiv:2403.15388*, 2024.
- Baifeng Shi, Boyi Li, Han Cai, Yao Lu, Sifei Liu, Marco Pavone, Jan Kautz, Song Han, Trevor Darrell, Pavlo Molchanov, et al. Scaling vision pre-training to 4k resolution. *arXiv preprint arXiv:2503.19903*, 2025a.
- Baifeng Shi, Boyi Li, Han Cai, Yao Lu, Sifei Liu, Marco Pavone, Jan Kautz, Song Han, Trevor Darrell, Pavlo Molchanov, et al. Scaling vision pre-training to 4k resolution. In *Proceedings of the Computer Vision and Pattern Recognition Conference*, pp. 9631–9640, 2025b.
- Amanpreet Singh, Vivek Natarjan, Meet Shah, Yu Jiang, Xinlei Chen, Devi Parikh, and Marcus Rohrbach. Towards VQA models that can read. In *Proceedings of the IEEE Conference on Computer Vision and Pattern Recognition*, pp. 8317–8326, 2019.
- Dingjie Song, Wenjun Wang, Shunian Chen, Xidong Wang, Michael X Guan, and Benyou Wang. Less is more: A simple yet effective token reduction method for efficient multi-modal llms. In *Proceedings of the 31st International Conference on Computational Linguistics*, pp. 7614–7623, 2025.
- Rhea Sanjay Sukthanker, Benedikt Staffler, Frank Hutter, and Aaron Klein. Large language model compression with neural architecture search. *arXiv preprint arXiv:2410.06479*, 2024.
- Gemini Team, Rohan Anil, Sebastian Borgeaud, Yonghui Wu, Jean-Baptiste Alayrac, Jiahui Yu, Radu Soricut, Johan Schalkwyk, Andrew M Dai, Anja Hauth, et al. Gemini: a family of highly capable multimodal models. *arXiv:2312.11805*, 2023.
- Piotr Teterwak, Soren Nelson, Nikoli Dryden, Dina Bashkurova, Kate Saenko, and Bryan A Plummer. Learning to compose superweights for neural parameter allocation search. In *Proceedings of the IEEE/CVF Winter Conference on Applications of Computer Vision*, pp. 2751–2760, 2024.
- Hugo Touvron, Thibaut Lavril, Gautier Izacard, Xavier Martinet, Marie-Anne Lachaux, Timothée Lacroix, Baptiste Rozière, Naman Goyal, Eric Hambro, Faisal Azhar, et al. Llama: Open and efficient foundation language models. *arXiv:2302.13971*, 2023.

-
- Vicuna. Vicuna: An open-source chatbot impressing gpt-4 with 90%* chatgpt quality. <https://vicuna.lmsys.org/>, 2023. Accessed: 2023.
- Peng Wang, Shuai Bai, Sinan Tan, Shijie Wang, Zhihao Fan, Jinze Bai, Keqin Chen, Xuejing Liu, Jialin Wang, Wenbin Ge, et al. Qwen2-vl: Enhancing vision-language model’s perception of the world at any resolution. *arXiv preprint arXiv:2409.12191*, 2024.
- Weihan Wang, Qingsong Lv, Wenmeng Yu, Wenyi Hong, Ji Qi, Yan Wang, Junhui Ji, Zhuoyi Yang, Lei Zhao, Xixuan Song, et al. CogVlm: Visual expert for pretrained language models. *arXiv:2311.03079*, 2023.
- Zichen Wen, Yifeng Gao, Shaobo Wang, Junyuan Zhang, Qintong Zhang, Weijia Li, Conghui He, and Linfeng Zhang. Stop looking for important tokens in multimodal language models: Duplication matters more. *arXiv preprint arXiv:2502.11494*, 2025.
- Yan Wu, Aoming Liu, Zhiwu Huang, Siwei Zhang, and Luc Van Gool. Neural architecture search as sparse supernet. In *Proceedings of the AAAI Conference on Artificial Intelligence*, volume 35, pp. 10379–10387, 2021.
- Long Xing, Qidong Huang, Xiaoyi Dong, Jiajie Lu, Pan Zhang, Yuhang Zang, Yuhang Cao, Conghui He, Jiaqi Wang, Feng Wu, et al. Pyramidrop: Accelerating your large vision-language models via pyramid visual redundancy reduction. *arXiv preprint arXiv:2410.17247*, 2024.
- Senqiao Yang, Yukang Chen, Zhuotao Tian, Chengyao Wang, Jingyao Li, Bei Yu, and Jiaya Jia. Visionzip: Longer is better but not necessary in vision language models. *arXiv preprint arXiv:2412.04467*, 2024.
- Linli Yao, Lei Li, Shuhuai Ren, Lean Wang, Yuanxin Liu, Xu Sun, and Lu Hou. DeCo: Decoupling token compression from semantic abstraction in multimodal large language models. *arXiv:2405.20985*, 2024.
- Qinghao Ye, Haiyang Xu, Guohai Xu, Jiabo Ye, Ming Yan, Yiyang Zhou, Junyang Wang, Anwen Hu, Pengcheng Shi, Yaya Shi, et al. mplug-owl: Modularization empowers large language models with multimodality. *arXiv:2304.14178*, 2023.
- Weihao Ye, Qiong Wu, Wenhao Lin, and Yiyi Zhou. Fit and prune: Fast and training-free visual token pruning for multi-modal large language models. *arXiv preprint arXiv:2409.10197*, 2024.
- Qizhe Zhang, Aosong Cheng, Ming Lu, Renrui Zhang, Zhiyong Zhuo, Jiajun Cao, Shaobo Guo, Qi She, and Shanghang Zhang. Beyond text-visual attention: Exploiting visual cues for effective token pruning in vlms. *arXiv preprint arXiv:2412.01818*, 2024a.
- Qizhe Zhang, Aosong Cheng, Ming Lu, Zhiyong Zhuo, MinQi Wang, Jiajun Cao, Shaobo Guo, Qi She, and Shanghang Zhang. [cls] attention is all you need for training-free visual token pruning: Make vlm inference faster. *arXiv preprint arXiv:2412.01818*, 2024b.
- Qizhe Zhang, Mengzhen Liu, Lichen Li, Ming Lu, Yuan Zhang, Junwen Pan, Qi She, and Shanghang Zhang. Beyond attention or similarity: Maximizing conditional diversity for token pruning in mllms. *arXiv preprint arXiv:2506.10967*, 2025.
- Yuan Zhang, Chun-Kai Fan, Junpeng Ma, Wenzhao Zheng, Tao Huang, Kuan Cheng, Denis Gudovskiy, Tomoyuki Okuno, Yohei Nakata, Kurt Keutzer, et al. Sparsevlm: Visual token sparsification for efficient vision-language model inference. *arXiv preprint arXiv:2410.04417*, 2024c.
- Long Zhao, Nitesh B Gundavarapu, Liangzhe Yuan, Hao Zhou, Shen Yan, Jennifer J Sun, Luke Friedman, Rui Qian, Tobias Weyand, Yue Zhao, et al. Videoprism: A foundational visual encoder for video understanding. *arXiv preprint arXiv:2402.13217*, 2024a.
- Yue Zhao, Long Zhao, Xingyi Zhou, Jialin Wu, Chun-Te Chu, Hui Miao, Florian Schroff, Hartwig Adam, Ting Liu, Boqing Gong, et al. Distilling vision-language models on millions of videos. In *Proceedings of the IEEE/CVF Conference on Computer Vision and Pattern Recognition*, pp. 13106–13116, 2024b.

-
- Yinmin Zhong, Shengyu Liu, Junda Chen, Jianbo Hu, Yibo Zhu, Xuanzhe Liu, Xin Jin, and Hao Zhang. {DistServe}: Disaggregating prefill and decoding for goodput-optimized large language model serving. In *18th USENIX Symposium on Operating Systems Design and Implementation (OSDI 24)*, pp. 193–210, 2024.
- Bin Zhu, Bin Lin, Munan Ning, Yang Yan, Jiayi Cui, HongFa Wang, Yatian Pang, Wenhao Jiang, Junwu Zhang, Zongwei Li, et al. Languagebind: Extending video-language pretraining to n-modality by language-based semantic alignment. *arXiv preprint arXiv:2310.01852*, 2023a.
- Deyao Zhu, Jun Chen, Xiaoqian Shen, Xiang Li, and Mohamed Elhoseiny. Minigpt-4: Enhancing vision-language understanding with advanced large language models. *arXiv:2304.10592*, 2023b.
- Jinguo Zhu, Weiyun Wang, Zhe Chen, Zhaoyang Liu, Shenglong Ye, Lixin Gu, Hao Tian, Yuchen Duan, Weijie Su, Jie Shao, et al. Internv13: Exploring advanced training and test-time recipes for open-source multimodal models. *arXiv preprint arXiv:2504.10479*, 2025.
- Barret Zoph and Quoc V Le. Neural architecture search with reinforcement learning. *arXiv preprint arXiv:1611.01578*, 2016.

A LLM USAGE

Large Language Models were used in this work solely as general-purpose assistance tools for minor editorial tasks, including grammar checking, basic text polishing to improve readability and academic writing style, and table formatting adjustments. LLMs did not play any significant role in research ideation, methodology development, experimental design, data analysis, or the primary writing of this manuscript. All technical contributions, scientific insights, experimental results, and core content originate entirely from the authors’ original research work. The authors take full responsibility for all content presented in this paper.

B ADDITIONAL RELATED WORKS

B.1 MULTIMODAL LARGE LANGUAGE MODEL (MLLM)

With the advancement of Large Language Models (LLMs) (Achiam et al., 2023; Touvron et al., 2023; Peng et al., 2023; Brown et al., 2020; Gunasekar et al., 2023; Abdin et al., 2024), Multimodal Large Language Models (MLLMs) (Liu et al., 2024b;a; Li et al., 2023b; Dai et al., 2023; Team et al., 2023; Bai et al., 2023a;b; Chen et al., 2023b; Ye et al., 2023; Du et al., 2021; Zhu et al., 2023b; Lin et al., 2023a; Liu et al., 2023a; Wang et al., 2023; Chen et al., 2023a; Zhao et al., 2024b; Abdin et al., 2024; Lin et al., 2023b) have successfully inherited the powerful reasoning capabilities of LLMs and extended them to multimodal tasks with visual inputs (Hudson & Manning, 2019; Li et al., 2023a; Chen et al., 2015; Fu et al., 2023; Liu et al., 2023b; Plummer et al., 2015; Agrawal et al., 2019; Lu et al., 2022). These models encode visual inputs as tokens to fully leverage LLM capabilities, mapping visual features extracted from visual encoders (Radford et al., 2021; Zhu et al., 2023a; Zhao et al., 2024a) into text embedding spaces through modality alignment and instruction fine-tuning.

However, these MLLMs feature excessive visual tokens, with most computation used for processing these tokens, predominantly occurring in the LLM decoder part as its parameter size usually far exceeds other components. For instance, LLaVA-1.5 (Liu et al., 2024b) converts a 336×336 image into 576 visual tokens, while LLaVA-NeXT (Liu et al., 2024a) generates 2,880 tokens from twice the resolution. This trend of increasing token usage has led to significantly higher computational costs, highlighting the growing need for efficient inference and eliminating redundant computations.

B.2 NEURAL ARCHITECTURE SEARCH (NAS)

While sharing some similarity with NAS (Zoph & Le, 2016; Liu et al., 2018; 2021; Wu et al., 2021; Sukthanker et al., 2024; Sarah et al., 2025; Teterwak et al., 2024), DOP is the extension of token reduction, not NAS. The key distinction is that NAS modifies network structure, while token reduction methods and our DOP both operate on input tokens, with DOP working at more fine-grained network

components. DOP can be viewed as fine-grained token pruning on local components. While DOP considers network structures for computational subdivision, these structures remain fixed. Similarly, prior progressive pruning methods (Ye et al., 2024; Xing et al., 2024; Zhang et al., 2024c) also leverage network structures (layer positions) for finer granularity. DOP’s optimization-based policy search is not exclusive to NAS and has been adopted in prior token pruning methods (Ye et al., 2024).

C METHOD DETAILS

C.1 SPARSE DIVERGENCE EVALUATION AND INTERPOLATION

We exploit the monotonically decreasing and smooth properties of \mathcal{D}_A , \mathcal{D}_P , and \mathcal{D}_v with respect to increasing d_A , d_P , and n_v . Instead of exhaustively evaluating all possible values for each of d_A , d_P , and n_v , we sample I key values per parameter, evaluate their individual divergences, and estimate remaining values via linear interpolation. For \mathcal{D}_A , the interpolated divergence is:

$$\hat{\mathcal{D}}_A(d_A) = \mathcal{D}_A(d_{A,i}) + \frac{d_A - d_{A,i}}{d_{A,i+1} - d_{A,i}} \cdot (\mathcal{D}_A(d_{A,i+1}) - \mathcal{D}_A(d_{A,i})) \quad (8)$$

where $d_{A,i}$ and $d_{A,i+1}$ are the nearest sampled values with $d_{A,i} \leq d_A \leq d_{A,i+1}$. The final number of divergence evaluations is reduced to $3 \cdot I$.

C.2 OUTPUT DIVERGENCE

We compute KL divergence between original and pruned model outputs to measure pruning impact. Specifically, we focus on the first output token generated during the prefilling stage. Given the original model’s output probability distribution $\mathbf{Pr}_{org} \in \mathbb{R}^V$ over vocabulary size V , we identify the top- k tokens and extract their probabilities:

$$\mathbf{X}_{top} = \arg \text{top-}k(\mathbf{Pr}_{org}), \quad \mathbf{p}_{org} = [\mathbf{Pr}_{org}[i]]_{i \in \mathbf{X}_{top}} \in \mathbb{R}^k \quad (9)$$

For a pruned model with policy $\mathbf{p}(\mathcal{P}) = [\mathbf{Pr}(\mathcal{P})[i]]_{i \in \mathbf{X}_{top}}$. We normalize both distributions for numerical stability as $\tilde{\mathbf{p}}_{org} = (\mathbf{p}_{org} + \epsilon) / \|\mathbf{p}_{org} + \epsilon\|_1$ and $\tilde{\mathbf{p}}(\mathcal{P}) = (\mathbf{p}(\mathcal{P}) + \epsilon) / \|\mathbf{p}(\mathcal{P}) + \epsilon\|_1$. We set $\epsilon = 10^{-8}$ and $k = 10$ in our implementation. The divergence is computed as:

$$\mathcal{D}(\mathcal{P}) = \mathcal{D}_{KL}(\tilde{\mathbf{p}}_{org} \parallel \tilde{\mathbf{p}}(\mathcal{P})) = \sum_{i=1}^k \tilde{\mathbf{p}}_{org}[i] \log \frac{\tilde{\mathbf{p}}_{org}[i]}{\tilde{\mathbf{p}}(\mathcal{P})[i]}. \quad (10)$$

C.3 THEORETICAL FLOPS

We calculate the theoretical FLOPs (TFLOPs) for MLLM decoder layers following the LLaMA architecture. For one layer with hidden size h , key/value feature dimension d , and MLP intermediate dimension m , the aTFLOPs can be expressed as:

$$\text{TFLOPs} = \underbrace{8n_Ahd + 4n_A^2d}_{\text{Multi-Head Attention}} + \underbrace{6n_Phm}_{\text{LLaMA-style MLP}} \quad (11)$$

where n_A and n_P denote the number of remaining tokens in MHA and MLP modules respectively. For architectures with different designs (e.g., Qwen), we adjust the calculations accordingly in our implementation. Note that n_A and n_P include not only visual tokens but also system, text, and output tokens. Some works may incorrectly consider only visual token counts when computing TFLOPs, leading to smaller TFLOPs calculations.

C.4 MINIMAL VISUAL TOKEN COUNT CONSTRAINT

Our ablation study in Section 5 reveals that different tasks have varying sensitivity to operation pruning. To ensure cross-task generalization, we perform policy optimization on the most sensitive OCR task. However, this occasionally creates another issue: without visual token count constraints, the optimized policy tends to be overly conservative with operations, primarily reducing tokens rather

than operations. This prevents the policy from fully utilizing its potential on tasks less sensitive to operation pruning, limiting overall performance.

To ensure better performance across all tasks, we add the minimal visual token count constraint $n_v \geq n_{\min}$. For determining n_{\min} , we make it adaptive to the given computation budget. Given budget τ , if reducing visual tokens alone to n_e exactly meets the computation budget, i.e., $\text{TFLOPs}(L, L, n_e) = \tau$ (if no exact n_e satisfies, we find the n_e that makes TFLOPs closest to τ), we set $n_{\min} = \alpha \cdot n_e$. In this paper, we set $\alpha = 1.5$ for LLaVA-series models (Liu et al., 2024b;a) and $\alpha = 1.25$ for other models (Bai et al., 2025; Zhu et al., 2025).

C.5 CROSS-MODEL DOP GENERALIZATION

As analyzed in Section 3.2.2, the most computationally expensive component of the optimization in Equation (7) is the validation runs required to evaluate individual divergences $\hat{D}_A(d_A)$, $\hat{D}_P(d_P)$, and $\hat{D}_v(n_v)$. In contrast, all other computations are negligible. These three divergences encapsulate the core information for our optimization, namely the distribution of operation and token redundancy within each model. Therefore, when transferring DOP to other models, we only need to transfer these three individual divergences $\hat{D}_A(d_A)$, $\hat{D}_P(d_P)$, and $\hat{D}_v(n_v)$.

Our transfer approach is based on rescaling the policy parameters d_A , d_P , and n_v according to the architectural differences between models, followed by interpolation to obtain individual divergences corresponding to feasible values on the target model.

Specifically, if our source model originally has N_v visual tokens and L decoder layers, while our target model has N'_v visual tokens and L' decoder layers, we rescale a policy (d_A, d_P, n_v) from the source model to obtain a corresponding policy (d'_A, d'_P, n'_v) on the target model:

$$d'_A = d_A \cdot \frac{L'}{L}, \quad d'_P = d_P \cdot \frac{L'}{L}, \quad n'_v = n_v \cdot \frac{N'_v}{N_v} \quad (12)$$

The corresponding individual divergences remain $\hat{D}_A(d_A)$, $\hat{D}_P(d_P)$, and $\hat{D}_v(n_v)$. However, (d'_A, d'_P, n'_v) may not represent a feasible policy since policy parameters must be integers, while d'_A , d'_P , and n'_v may not be integers. Therefore, based on the rescaled points and their corresponding individual divergences, we perform interpolation identical to that described in Section C.1 to obtain individual divergences for feasible policies on the target model. Finally, we substitute these transferred individual divergences into Equation (7) and apply the target model’s parameters to compute TFLOPs and token count constraints, thereby obtaining DOP policies for the target model.

D EXPERIMENTAL SETUP DETAILS

D.1 MLLM MODEL DETAILS

LLaVA-1.5 (Liu et al., 2024b) is a prominent open-source multimodal large language model combining a CLIP visual encoder (Radford et al., 2021) with the Vicuna language model (Vicuna, 2023) through a linear projection layer. LLaVA-1.5 enhances the original architecture with a multi-layer perceptron projection, higher resolution inputs (336×336 pixels generating 576 visual tokens), and diverse instruction-following training data. Common variants include 7B and 13B parameter versions based on corresponding Vicuna backbones.

LLaVA-NeXT (Liu et al., 2024a) (also known as LLaVA-1.6) adopts an adaptive resolution strategy that dynamically adjusts input dimensions based on each image’s native aspect ratio, scaling up to 4× the baseline resolution. High-resolution images are partitioned into sub-regions matching the original input size, processed independently, then concatenated for language model input. This enhances visual reasoning, OCR, and world knowledge capabilities. Following CDPruner (Zhang et al., 2025) for fair comparison, we fix input resolution at 672×672 pixels (4× increase), generating 2,880 visual tokens per image.

Qwen2.5-VL (Bai et al., 2025) is a state-of-the-art open-source multimodal model from the Qwen-VL family, offering substantial improvements in visual comprehension, document analysis, and video processing over Qwen2-VL (Wang et al., 2024). The architecture features an enhanced Vision

Transformer with window attention, SwiGLU activation, and RMSNorm components consistent with the Qwen2.5 language model. A key innovation is adaptive resolution handling that controls visual token counts through input image resizing. Following CDPruner (Zhang et al., 2025), we fix baseline resolution at 1008×1008 pixels (1296 visual tokens), with both Resizing baselines and DOP_R controlling token counts through image resizing.

InternVL3 (Zhu et al., 2025) is a state-of-the-art open-source multimodal model that maintains the ViT-MLP-LLM framework connecting a Vision Transformer to a language model via an MLP bridge. Key innovations include Variable Visual Position Encoding for handling extensive multimodal sequences and unified multimodal pre-training that simultaneously develops linguistic and visual-linguistic competencies. The model achieves exceptional performance across diverse applications including tool integration, GUI agents, and industrial image analysis. Following CDPruner (Zhang et al., 2025), we use 896×896 input resolution (1280 visual tokens) as the 100% TFLOPs baseline, with Resizing baselines and DOP_R controlling token counts through resolution adjustment.

D.2 BENCHMARK DETAILS

VQAv2 (Goyal et al., 2017) is an open-ended visual question answering benchmark that assesses models’ integration of visual perception, linguistic comprehension, and commonsense reasoning. The dataset contains 265,016 images from COCO (Chen et al., 2015) and synthetic abstract scenes, with approximately 5.4 questions per image. Each question includes 10 verified correct answers and 3 plausible incorrect alternatives. We evaluate on the test-dev partition.

GQA (Hudson & Manning, 2019) is a comprehensive open-ended visual question answering dataset constructed from Visual Genome images (Krishna et al., 2017), designed to evaluate compositional reasoning and visual comprehension. The benchmark contains over 22 million balanced question-answer pairs, with each image annotated with detailed scene graphs specifying object categories, attributes, and relationships. We evaluate on the test-dev balanced partition.

VizWiz (Gurari et al., 2018) is a visual question answering dataset collected from real-world accessibility scenarios, where blind users captured images and posed spoken questions about their content. Each visual inquiry is paired with 10 crowd-sourced responses, with evaluation focusing on answering visual questions and determining when questions are unanswerable from the available visual information. The benchmark emphasizes real-world challenges including poor image quality and unclear visual content that complicate automated understanding. We evaluate on the test partition.

ScienceQA (Saikh et al., 2022) is a comprehensive multimodal multiple-choice dataset for evaluating scientific reasoning across natural science, language science, and social science domains. The benchmark contains 21,208 questions organized into 26 topics, 127 categories, and 379 skills, with 48.7% including images, 48.2% including text, and 30.8% combining both modalities. Most questions provide educational resources including grounded lectures (83.9%) and detailed explanations (90.5%). We evaluate on the test split containing image-based questions, referred to as SQA¹.

SeedBench (Li et al., 2023a) is a multiple-choice evaluation framework for MLLMs featuring 19,242 human-verified questions across 12 assessment dimensions for spatial (image) and temporal (video) understanding. The benchmark covers nine spatial dimensions including scene understanding, instance identity, attributes, location, counting, spatial relations, interactions, visual reasoning, and text recognition, plus three temporal dimensions for video analysis. We focus on the 14,233 image-based questions spanning the nine spatial dimensions, referred to as Seed¹.

POPE (Li et al., 2023c) is a benchmark designed to measure object hallucination in large vision-language models using COCO images (Chen et al., 2015). The dataset focuses on simple yes/no questions about whether specific objects appear in each image, allowing evaluation of how often models incorrectly claim to see absent objects. The benchmark uses precision, recall, and F1 score as evaluation metrics. We evaluate on the test split.

MME (Fu et al., 2023) is a comprehensive evaluation framework that assesses both perception and cognition capabilities of multimodal large language models through 14 subtasks. The perception component evaluates visual recognition from coarse-grained tasks (object presence, counting, positioning, color) to fine-grained recognition (posters, celebrities, scenes, landmarks, artworks) and

OCR capabilities. The cognition component tests higher-level reasoning through commonsense reasoning, numerical calculations, text translation, and code reasoning.

MMBench (Liu et al., 2023b) is a comprehensive evaluation framework that assesses vision-language capabilities through an extensive and diverse collection of evaluation questions. A key innovation is the CircularEval strategy, which uses ChatGPT to transform open-ended model responses into structured multiple-choice formats for more consistent evaluation. The benchmark is available in English (MMB) and Chinese (MMB^{CN}) versions.

TextVQA (Singh et al., 2019) is a benchmark that tests models’ ability to read and understand text embedded within images. The dataset draws from Open Images v3 (Krasin et al., 2017) and features diverse real-world scenarios including signs, billboards, and product packaging containing textual information. The benchmark requires integration of optical character recognition (OCR) capabilities with visual reasoning skills for successful multimodal comprehension. We evaluate on the validation split and optimize DOP policies using samples from the training split.

AI2D (Kembhavi et al., 2016) is a diagram-based question answering benchmark focusing on scientific visual reasoning using grade school science materials. The dataset contains over 5,000 science diagrams with more than 150,000 structured annotations and over 15,000 multiple-choice questions, creating opportunities for research in visual reasoning and diagram comprehension within scientific domains. We evaluate on the test split with mask.

ChartQA (Masry et al., 2022) is a large-scale benchmark evaluating question answering over charts, requiring complex reasoning that combines visual interpretation with logical and arithmetic operations. The dataset includes 9.6K human-written questions and 23.1K questions generated from chart summaries. ChartQA requires models to perform multistep reasoning using both visual chart content and underlying data tables, demonstrating the need for sophisticated multimodal understanding. We evaluate on the test split.

OCRBench (Liu et al., 2024c) is a comprehensive evaluation framework that measures optical character recognition capabilities of large multimodal models across diverse text-related visual tasks. The benchmark encompasses 29 datasets covering text recognition, scene text-focused VQA, document-oriented VQA, key information extraction, and handwritten mathematical expression recognition.

D.3 BASELINE DETAILS

FastV (Chen et al., 2024) is the first work to identify redundant visual attention in multimodal large language models, addressing this through a pruning strategy that removes visual tokens with the lowest visual-text attention scores after the second layer for training-free inference acceleration.

PyramidDrop (Xing et al., 2024) is a progressive pruning method extending FastV’s insights by observing that visual token pruning in earlier layers significantly affects performance, while token redundancy becomes more pronounced at deeper layers. The method introduces multi-stage hierarchical pruning that partitions the MLLM into phases, systematically removing a predetermined fraction of visual tokens at each stage boundary.

FitPrune (Ye et al., 2024) is a progressive pruning method advancing FastV by investigating optimal timing and methodology for visual token pruning. The approach employs binary search to maintain visual-text attention distribution as closely as possible to the original under computational budgets, deriving an optimal pruning configuration. Visual tokens are then removed according to this strategy to maximize retention of original model capabilities.

SparseVLM (Zhang et al., 2024c) is a progressive token pruning approach that distinguishes itself by examining instruction tokens’ role in vision-language attention mechanisms. The method argues that textual tokens contribute unequally to visual token pruning decisions, with only those highly correlated with visual content being significant. SparseVLM first identifies text tokens most relevant to visual input as evaluators, then leverages their attention patterns toward visual tokens to direct pruning, achieving enhanced performance.

LLaVA-Prumerge (Shang et al., 2024) pioneers token pruning based exclusively on visual information and token merging. The method identifies significant visual tokens using attention scores from the visual encoder, then merges each remaining token with its most semantically similar to-

ken through clustering techniques. LLaVA-Prumerge+ extends this framework by incorporating spatially uniform sampling for additional performance enhancements.

VisionZip (Yang et al., 2024) shares similarities with LLaVA-Prumerge in utilizing visual information for token pruning decisions. The method observes that visual encoder attention exhibits high concentration patterns and leverages this to extract dominant tokens based on visual attention weights. VisionZip then applies clustering to identify contextual tokens from the remaining pool, combining both groups before feeding them into the language model to maximize visual information preservation.

VisPruner (Zhang et al., 2024a) uses visual information for token pruning by identifying limitations in existing text-visual attention-based approaches and implementing a dual-phase strategy combining visual attention-based selection of significant tokens with similarity-based duplicate removal to maximize retention of diverse visual information.

TRIM (Song et al., 2025) addresses the limitation that pruning based solely on visual information while disregarding user instructions may result in suboptimal performance. The method incorporates CLIP metrics by calculating cosine similarity between image tokens from the visual encoder and text tokens from the text encoder, using these similarity measures to assess visual token significance. Visual tokens with lower similarity scores are eliminated to achieve inference acceleration.

DART (Wen et al., 2025) proposes that token duplication presents a more critical concern than token importance in pruning strategies. The method begins by identifying a small collection of pivot tokens, then iteratively preserves the most diverse tokens by selecting those with minimal similarity to previously chosen tokens. This process yields maximally diverse visual tokens for downstream processing.

DivPrune (Alvar et al., 2025) also emphasizes token diversity but reformulates the token pruning challenge as a Max-Min Diversity Problem (MMDP). The method retains the most diverse token subset by maximizing the minimum pairwise distance among selected tokens, providing a mathematically principled approach to diversity optimization.

CDPruner (Zhang et al., 2025) addresses limitations in existing methods by introducing conditional diversity maximization for visual token pruning. Unlike attention-based approaches that retain duplicate tokens or similarity-based methods that ignore instruction relevance, CDPruner defines conditional similarity between visual tokens given instruction context and reformulates pruning as a determinantal point process (DPP) optimization. This training-free approach achieves current state-of-the-art performance across multiple models and benchmarks.

D.4 CONFIGURATION DETAILS

D.4.1 BASELINE CONFIGURATIONS ON LLaVA

For experiments on the LLaVA model, we evaluated our approach against several state-of-the-art methods including FastV, PyramidDrop, FitPrune, SparseVLM, LLaVA-Prumerge, VisionZip, VisPruner, TRIM, DART, DivPrune, and CDPruner. To ensure fair comparison and minimize implementation-induced variations, we adopted the performance metrics reported in Zhang et al. (2024a; 2025) for methods evaluated at comparable TFLOPs ratios across standard benchmarks: VQAv2, GQA, VizWiz, ScienceQA, POPE, MME, MMBench (both English and Chinese variants), TextVQA, AI2D, ChartQA, and OCRBench.

For FitPrune, we conducted independent evaluation using its official implementation on LLaVA-1.5-7B, optimizing on the same validation set and assessing performance across all benchmarks to maintain experimental consistency. Since Zhang et al. (2024a; 2025) did not report baseline performance on SeedBench, we implemented and evaluated all baselines on this benchmark using their official implementations.

D.4.2 BASELINE CONFIGURATIONS ON QWEN2.5-VL AND INTERNVL3

We followed the evaluation protocol established in Zhang et al. (2025) using VLMEvalKit. However, since Zhang et al. (2025) has not released their official implementations and several critical implementation details remain unclear, which could lead to significant reproduction discrepancies,

Model	L	N_v	d_A & d_P (sampled)	n_v (sampled)
LLaVA-1.5-7B	32	576	{26, 20, 14, 8, 4, 0}	{512, 256, 128, 64, 32, 16}
LLaVA-1.5-13B	40	576	{32, 24, 16, 8, 4, 0}	{512, 256, 128, 64, 32, 16}
LLaVA-Next-7B	32	2880	{26, 20, 14, 8, 4, 0}	{2560, 1280, 640, 320, 160, 80}
LLaVA-Next-13B	40	2880	{32, 24, 16, 8, 4, 0}	{2560, 1280, 640, 320, 160, 80}
Qwen2.5-VL-7B	28	1296	{23, 18, 13, 8, 4, 0}	{512, 256, 128, 64, 32, 16}
InternVL3-8B	28	1008	{23, 18, 13, 8, 4, 0}	{512, 256, 128, 64, 32, 16}

Table 6: Sampling points for evaluating individual divergence. L : number of decoder layers; N_v : visual token count at 100% TFLOPs; d_A and d_P : we sample identical sets for MHA depth d_A and MHA depth d_P ; n_v is visual token counts.

we opted to directly adopt the reported results for FastV, DivPrune, and CDPruner from Zhang et al. (2025).

We conducted our own evaluations of Resizing and DOP_R based on VLMEvalKit, ensuring alignment with the documented specifications. Specifically, for Qwen2.5-VL-7B, we established the baseline configuration by fixing the input pixel count at 1,016,064, yielding 1,296 visual tokens as the 100% TFLOPs reference. For different resizing configurations, we set the input pixel count to $\#\text{visual tokens} \times 784$. Correspondingly, for 512, 256, and 128 visual tokens, we configured the input pixel counts to 401,408, 200,704, and 100,352, respectively. For InternVL3-8B, we adopted the same resizing methodology.

D.4.3 DOP CONFIGURATIONS

DOP exclusively prunes image token operations and performs optimization once on 100 randomly selected TextVQA training samples with random seed 42. In most experiments, we conducted “model-specific” optimization, where each model undergoes optimization once, and the resulting policy is applied consistently across all benchmarks at the same TFLOPs ratio.

For the divergence terms $\hat{\mathcal{D}}_A(d_A)$, $\hat{\mathcal{D}}_P(d_P)$, and $\hat{\mathcal{D}}_v(n_v)$ in Equation (7), we sample $K = 6$ points each for visual token count, MHA depth, and MLP depth to evaluate output divergence. These sampling points are detailed in Table 6. We set n_{min} according to Section C.4.

For LLaVA-series models, we evaluate DOP_V and DOP_{CD} , corresponding to VisPruner and CDPruner respectively as token reduction methods. For Qwen2.5-VL and InternVL3, we evaluate DOP_R with input image resizing as the token reduction approach.

D.4.4 IMPLEMENTATION DETAILS

For LLaVA model experiments, we implemented DOP_V using VisPruner’s official codebase¹ and developed DOP_{CD} based on CDPruner’s official implementation² to eliminate potential variations caused by implementation differences. For Qwen2.5-VL and InternVL3 evaluations, we adopted the same approach as CDPruner by utilizing VLMEvalKit³ for evaluation.

E ADDITIONAL EXPERIMENTS

E.1 DIVERGENCE RANKING CORRELATION ANALYSIS FOR ADDITIVE APPROXIMATION

Section 3.2.2 uses an additive approximation to reduce optimization complexity by replacing the joint divergence $\mathcal{D}(d_A, d_P, n_v)$ in Equation (5) with the sum of three individual divergences:

$$\mathcal{D}_{\text{sum}}(d_A, d_P, n_v) = \mathcal{D}_A(d_A) + \mathcal{D}_P(d_P) + \mathcal{D}_v(n_v) = \mathcal{D}(d_A, L, N_v) + \mathcal{D}(L, d_P, N_v) + \mathcal{D}(L, L, n_v)$$

The key to ensuring sufficiently accurate optimization is that $\mathcal{D}_{\text{sum}}(d_A, d_P, n_v)$ preserves the sufficiently accurate ranking order of $\mathcal{D}(d_A, d_P, n_v)$, allowing Equation (6) to largely hold.

¹<https://github.com/Theia-4869/VisPruner>

²<https://github.com/Theia-4869/CDPruner>

³<https://github.com/open-compass/VLMEvalKit>

Model	Spearman’s ρ	p -value
LLaVA-1.5-7B	0.799	4.19×10^{-49}
LLaVA-Next-7B	0.862	3.94×10^{-65}

Table 7: Spearman’s rank correlation between joint divergence $\mathcal{D}(d_A, d_P, n_v)$ and additive approximation $\mathcal{D}_{\text{sum}}(d_A, d_P, n_v)$ across 216 sampled combinations.

We validate this by computing that rankings based on \mathcal{D} and \mathcal{D}_{sum} are highly correlated using Spearman’s rank correlation coefficient. Specifically, we sample combinations of (d_A, d_P, n_v) and evaluate both $\mathcal{D}(d_A, d_P, n_v)$ and $\mathcal{D}_{\text{sum}}(d_A, d_P, n_v)$ on real MLLM models with validation tasks, then rank the sampled combinations according to $\mathcal{D}(d_A, d_P, n_v)$ and $\mathcal{D}_{\text{sum}}(d_A, d_P, n_v)$ respectively and compute the Spearman’s rank correlation coefficient between these two rankings.

We conduct this experiment on LLaVA-1.5-7B and LLaVA-Next-7B with evaluating divergence on the same 100 TextVQA samples as other experiments. For d_A and d_P , we sample $I = 6$ points each: $\mathcal{S}_d = \{26, 20, 14, 8, 4, 0\}$ for both models. For n_v , we use $\mathcal{S}_v^{1.5} = \{512, 256, 128, 64, 32, 16\}$ for LLaVA-1.5-7B and $\mathcal{S}_v^{\text{Next}} = \{2560, 1280, 640, 320, 160, 80\}$ for LLaVA-Next-7B.

We evaluate $\mathcal{D}(d_A, d_P, n_v)$ for all combinations in $\mathcal{C} = \mathcal{S}_d \times \mathcal{S}_d \times \mathcal{S}_v$, yielding $|\mathcal{C}| = 6^3 = 216$ points. For individual divergences, we evaluate $\mathcal{D}_A(d_A)$ for $d_A \in \mathcal{S}_d$, $\mathcal{D}_P(d_P)$ for $d_P \in \mathcal{S}_d$, and $\mathcal{D}_v(n_v)$ for $n_v \in \mathcal{S}_v$, then sum these to obtain $\mathcal{D}_{\text{sum}}(d_A, d_P, n_v)$ for all combinations in \mathcal{C} . Let $\mathcal{R}_{\mathcal{D}}$ and \mathcal{R}_{sum} denote the rankings of the combinations based on \mathcal{D} and \mathcal{D}_{sum} respectively. The Spearman’s rank correlation coefficient without tied ranks is computed as:

$$\rho = 1 - \frac{6 \sum_{i=1}^{|\mathcal{C}|} (\mathcal{R}_{\mathcal{D}}(i) - \mathcal{R}_{\text{sum}}(i))^2}{|\mathcal{C}|(|\mathcal{C}|^2 - 1)}$$

where $|\mathcal{C}| = 216$. When tied ranks exist, the calculation becomes more complex, and we use the implemented function in `scipy`⁴ which automatically handles such cases.

Table 7 shows strong and highly significant monotonic relationships between the additive proxy and joint divergence on both models ($\rho \geq 0.799$, $p < 10^{-48}$). The additive approximation \mathcal{D}_{sum} closely preserves the ranking induced by joint divergence \mathcal{D} , validating our substitution of \mathcal{D} with \mathcal{D}_{sum} for reduced optimization complexity. While rankings between a small number of combinations may occasionally swap, the approximation is sufficiently accurate across different models.

E.2 FULL COMPARISON ON LLaVA

Tables 8 to 11 present comprehensive evaluations of DOP on LLaVA-1.5-7B&13B and LLaVA-Next-7B&13B across three different TFLOPs ratios, along with comparisons against 11 baseline methods. The results demonstrate that at relatively high TFLOPs ratios, progressive pruning methods such as FitPrune, PDrop, and SparseVLM indeed exhibit certain advantages. However, at low TFLOPs ratios, their performance deteriorates rapidly, whereas our DOP consistently improves performance across all TFLOPs ratios.

E.3 FULL COMPARISON ON QWEN2.5-VL AND INTERNVL3

Table 12 presents full evaluation of DOP across three different TFLOPs ratios on Qwen2.5-VL-7B, while Table 13 shows complete evaluation results across two different TFLOPs ratios on InternVL3-8B. The results reveal that across different TFLOPs ratios, CDPruner and DivPrune struggle to outperform basic FastV and Resizing baselines, which stands in stark contrast to their significant advantages on LLaVA models, raising concerns about overfitting to model-specific patterns. In contrast, DOP maintains consistent gains across architectures, indicating that different architectures share similar structural redundancy patterns and enabling strong cross-model generalization.

Method	VQA ^{v2}	GQA	VizWiz	SQA ^I	Seed ^I	VQA ^{Text}	POPE	MME	MMB	MMB ^{CN}	Rel. Avg.
<i>Upper Bound: 100% TFLOPs (= 576 Visual Tokens Every Layer)</i>											
LLaVA-1.5-7B	78.5	61.9	50.1	69.5	66.2	58.2	85.9	1506.5	64.7	58.1	100%
<i>Retain 37% TFLOPs (= 128 Visual Tokens Every Layer)</i>											
FastV (Chen et al., 2024)	71.0	54.0	51.9	69.2	55.9	56.4	68.2	1368.9	63.0	55.9	92.6%
PDrop (Xing et al., 2024)	74.3	57.1	49.4	70.1	54.8	56.7	77.5	1444.1	62.3	55.3	94.4%
FitPrune (Ye et al., 2024)	72.9	58.5	51.7	68.0	62.2	55.7	77.9	1445.3	62.7	56.2	95.8%
SparseVLM (Zhang et al., 2024c)	75.1	57.3	49.7	69.0	58.2	56.3	83.1	1399.3	62.6	56.9	95.6%
PruMerge+ (Shang et al., 2024)	75.0	58.2	53.7	69.1	62.7	54.0	83.1	1408.1	61.8	55.8	96.5%
TRIM (Song et al., 2025)	75.4	58.4	51.6	68.6	62.5	52.2	85.3	1413.4	63.0	52.3	95.7%
VisionZip (Yang et al., 2024)	75.6	57.6	51.6	68.7	61.8	56.9	83.3	1436.9	62.1	57.0	96.9%
DART (Wen et al., 2025)	74.7	57.9	52.8	69.1	62.2	56.3	80.4	1408.7	60.7	57.3	96.4%
DivPrune (Alvar et al., 2025)	76.0	59.4	52.8	68.6	63.6	55.9	87.0	1405.1	61.5	54.8	97.3%
VisPruner (Zhang et al., 2024a)	75.8	58.2	52.7	69.1	62.5	57.0	84.6	1461.4	62.7	57.3	97.9%
DOP_V (Ours)	76.9	59.3	52.3	69.1	63.4	57.4	85.9	1447.8	63.1	57.2	98.4%
CDPruner (Zhang et al., 2025)	76.6	59.9	52.8	69.0	64.0	56.2	87.7	1431.4	63.1	55.0	98.2%
DOP_{CD} (Ours)	77.2	60.5	52.8	68.7	64.8	57.1	87.6	1448.1	63.3	55.5	98.8%
<i>Retain 28% TFLOPs (= 64 Visual Tokens Every Layer)</i>											
FastV (Chen et al., 2024)	55.9	46.0	49.1	70.1	51.9	51.6	35.5	973.5	50.1	42.1	76.7%
PDrop (Xing et al., 2024)	56.3	46.1	46.3	68.8	48.9	49.2	40.8	982.2	48.0	36.6	74.6%
FitPrune (Ye et al., 2024)	63.7	52.3	51.1	68.0	55.8	51.2	73.6	1287.5	58.5	49.7	88.5%
SparseVLM (Zhang et al., 2024c)	66.9	52.0	49.4	69.2	52.2	52.1	69.7	1190.4	58.3	49.6	87.1%
PruMerge+ (Shang et al., 2024)	71.3	55.4	53.7	69.5	60.3	52.0	75.7	1316.8	59.6	52.1	92.5%
TRIM (Song et al., 2025)	72.4	56.6	51.1	69.0	61.0	49.7	85.9	1350.9	60.9	48.2	92.9%
VisionZip (Yang et al., 2024)	72.4	55.1	52.9	69.0	60.0	55.5	77.0	1365.2	60.1	55.4	94.1%
DART (Wen et al., 2025)	71.3	54.7	53.5	69.3	59.6	54.7	73.8	1365.1	59.5	54.0	93.1%
DivPrune (Alvar et al., 2025)	74.1	57.5	53.6	68.0	61.7	54.5	85.5	1334.7	60.1	52.3	95.0%
VisPruner (Zhang et al., 2024a)	72.7	55.4	53.3	69.1	58.5	55.8	80.4	1369.9	61.3	55.1	94.6%
DOP_V (Ours)	74.6	57.1	53.6	69.2	60.3	56.5	83.1	1394.6	61.6	56.5	96.4%
CDPruner (Zhang et al., 2025)	75.4	58.6	53.4	68.1	62.5	55.3	87.5	1415.1	61.1	53.2	96.7%
DOP_{CD} (Ours)	76.2	59.6	53.4	68.3	63.6	55.8	87.6	1436.3	62.4	55.1	97.9%
<i>Retain 23% TFLOPs (= 32 Visual Tokens Every Layer)</i>											
PruMerge+ (Shang et al., 2024)	65.6	52.9	53.5	67.9	55.4	49.2	66.7	1236.6	55.1	45.9	86.6%
TRIM (Song et al., 2025)	68.6	54.5	50.7	68.1	58.6	47.6	84.9	1251.8	57.7	40.1	88.5%
VisionZip (Yang et al., 2024)	67.1	51.8	52.4	69.1	56.2	53.1	69.4	1251.2	57.0	50.3	88.8%
DART (Wen et al., 2025)	67.1	52.9	52.5	69.3	58.4	52.2	69.1	1273.3	58.5	50.0	89.5%
DivPrune (Alvar et al., 2025)	71.2	54.9	53.3	68.6	58.7	52.9	81.5	1284.9	57.6	49.1	91.8%
VisPruner (Zhang et al., 2024a)	67.7	52.2	53.0	69.2	54.3	53.9	72.7	1271.0	58.4	52.7	90.1%
DOP_V (Ours)	71.0	54.8	53.9	69.1	56.7	54.5	79.6	1306.5	59.4	53.7	92.9%
CDPruner (Zhang et al., 2025)	73.6	57.0	53.1	69.5	60.9	53.2	87.9	1373.0	59.6	49.6	94.6%
DOP_{CD} (Ours)	74.7	58.1	53.6	69.3	62.2	54.2	87.9	1397.5	60.1	52.2	96.1%
<i>Lower Bound: Retain 18.6% TFLOPs (= 0 Visual Token)</i>											

Table 8: **Performance comparison on LLaVA-1.5-7B (Liu et al., 2024b) under different computation budgets.** We evaluate across 10 benchmarks: VQAv2, GQA (Hudson & Manning, 2019), VizWiz, SQA-Img, SeedBench (Li et al., 2023a), TextVQA, POPE (Li et al., 2023c), MME (Fu et al., 2023), MMBench (Liu et al., 2023b), and MMB-CN. We report accuracy (%) for most benchmarks. Avg. represents the mean performance ratio relative to Vanilla across all benchmarks (higher is better). **Bold** values indicate the best performances in each setting. DOP_V uses VisPruner to reduce visual tokens, while DOP_{CD} uses CDPruner. DOP consistently outperforms all baselines with policies only optimized on a subset of only 100 TextVQA training set samples. Lower Bound indicates the minimum possible computation in our settings. Our comparison matches actual TFLOPs and notes the per-layer token counts that achieve these TFLOPs.

Method	VQA ^{v2}	GQA	VizWiz	SQA ¹	Seed ¹	VQA ^{Text}	POPE	MME	MMB	MMB ^{CN}	Rel. Avg.
<i>Upper Bound: 100% TFLOPs (= 576 Visual Tokens Every Layer)</i>											
LLaVA-1.5-13B	80.0	63.3	53.6	72.8	68.3	61.2	86.0	1531.2	68.5	63.5	100%
<i>Retain 37% TFLOPs (= 128 Visual Tokens Every Layer)</i>											
FastV (Chen et al., 2024)	75.3	58.3	54.6	74.2	63.2	58.6	75.5	1460.6	66.1	62.3	95.6%
PDrop (Xing et al., 2024)	78.2	61.0	53.8	73.3	65.6	60.2	83.6	1489.5	67.5	62.8	98.2%
SparseVLM (Zhang et al., 2024c)	77.6	59.6	51.4	74.3	64.5	59.3	85.0	1487.9	68.4	62.6	97.5%
PruMerge+ (Shang et al., 2024)	76.2	58.3	52.8	73.3	63.8	56.1	82.7	1445.9	66.3	61.2	95.5%
TRIM (Song et al., 2025)	76.4	59.4	49.7	72.4	64.5	55.0	86.8	1426.9	67.1	58.4	95.0%
VisionZip (Yang et al., 2024)	76.8	57.9	52.3	73.8	63.7	58.9	82.7	1449.2	67.4	62.5	96.4%
DART (Wen et al., 2025)	75.7	57.7	53.0	74.2	62.9	58.7	80.4	1395.0	65.4	62.2	95.3%
DivPrune (Alvar et al., 2025)	77.1	59.2	53.5	72.8	64.4	58.0	86.8	1457.7	66.3	60.7	96.7%
VisPruner (Zhang et al., 2024a)	76.9	58.2	53.0	74.3	63.6	58.9	84.1	1449.7	67.3	62.5	96.8%
DOP_V (Ours)	78.1	59.3	53.4	73.6	65.1	59.1	85.4	1461.7	67.2	63.1	97.6%
CDPruner (Zhang et al., 2025)	77.7	59.7	52.9	73.2	65.1	58.4	87.3	1478.0	67.5	61.5	97.5%
DOP_{CD} (Ours)	78.3	59.8	53.1	73.0	66.0	58.6	86.5	1490.7	67.5	62.2	97.9%
<i>Retain 28% TFLOPs (= 64 Visual Tokens Every Layer)</i>											
FastV (Chen et al., 2024)	65.3	51.9	53.8	73.1	56.1	53.4	56.9	1246.4	59.2	55.1	85.5%
PDrop (Xing et al., 2024)	70.8	54.1	50.5	73.1	58.4	55.3	66.1	1247.0	63.1	56.6	88.4%
SparseVLM (Zhang et al., 2024c)	73.2	55.9	52.1	73.0	60.3	57.1	77.9	1374.3	65.2	60.3	92.9%
PruMerge+ (Shang et al., 2024)	72.6	56.3	52.4	73.5	60.7	54.4	75.7	1338.2	65.0	59.3	92.0%
TRIM (Song et al., 2025)	73.2	57.9	49.2	72.0	62.5	52.0	86.5	1406.2	65.0	52.7	92.0%
VisionZip (Yang et al., 2024)	73.7	56.2	53.2	74.2	60.6	57.4	75.7	1379.6	64.9	61.3	93.4%
DART (Wen et al., 2025)	72.4	55.7	53.4	73.8	60.1	57.3	72.8	1380.0	64.7	60.6	92.6%
DivPrune (Alvar et al., 2025)	75.2	57.9	54.4	71.7	62.5	57.4	84.5	1454.2	64.1	59.8	95.2%
VisPruner (Zhang et al., 2024a)	73.8	56.4	53.9	74.0	60.4	58.1	79.7	1376.2	64.4	60.0	93.8%
DOP_V (Ours)	75.7	57.3	53.7	73.4	62.6	58.5	81.1	1414.4	66.8	62.0	95.5%
CDPruner (Zhang et al., 2025)	76.7	59.4	53.6	72.5	64.1	57.6	87.1	1466.8	65.5	58.8	96.3%
DOP_{CD} (Ours)	77.2	59.5	52.8	72.4	64.6	57.7	87.0	1484.8	66.9	60.8	96.9%
<i>Retain 23% TFLOPs (= 32 Visual Tokens Every Layer)</i>											
PruMerge+ (Shang et al., 2024)	66.8	54.1	52.3	71.7	57.8	52.4	67.4	1269.1	61.1	53.5	87.0%
TRIM (Song et al., 2025)	69.8	55.6	48.8	70.4	59.3	49.6	85.8	1284.7	63.1	45.4	87.8%
VisionZip (Yang et al., 2024)	68.4	52.7	53.0	72.9	56.2	55.2	66.8	1257.7	61.2	55.8	87.7%
DART (Wen et al., 2025)	68.1	53.9	52.0	73.2	57.6	55.1	66.9	1282.8	61.9	56.2	88.3%
DivPrune (Alvar et al., 2025)	72.0	56.2	54.5	70.9	60.1	54.6	79.3	1405.2	61.7	57.2	91.9%
VisPruner (Zhang et al., 2024a)	69.0	52.6	52.8	71.7	56.5	56.0	71.9	1314.2	61.3	56.1	88.8%
DOP_V (Ours)	73.2	56.0	53.8	73.6	59.7	57.2	78.8	1365.6	64.3	59.5	93.1%
CDPruner (Zhang et al., 2025)	75.2	58.5	53.5	71.9	62.5	55.3	87.6	1421.0	63.7	56.6	94.4%
DOP_{CD} (Ours)	76.2	59.0	54.7	68.9	63.8	56.7	87.5	1468.9	65.1	58.7	95.6%
<i>Lower Bound: Retain 18.6% TFLOPs (= 0 Visual Token)</i>											

Table 9: **Performance on LLaVA-1.5-13B under different computation budgets.** We evaluate across 10 benchmarks: We evaluate across 10 benchmarks: VQA^{V2} (Goyal et al., 2017), VizWiz (Gurari et al., 2018), SQA¹ (Saikh et al., 2022), GQA (Hudson & Manning, 2019), Seed¹ (Li et al., 2023a), MME (Fu et al., 2023), MMB (Liu et al., 2023b), POPE (Li et al., 2023c), MMB^{CN} and VQA^{Text} (Singh et al., 2019). We report accuracy (%) for most benchmarks. Avg. represents the mean performance ratio relative to Vanilla across all benchmarks (higher is better). **Bold** values indicate the best performances in each setting. DOP_V uses VisPruner to reduce visual tokens, while DOP_{CD} uses CDPruner. DOP consistently outperforms all baselines with policies only optimized on a subset of only 100 TextVQA training set samples. Lower Bound indicates the minimum possible computation in our settings. Our comparison matches actual TFLOPs and notes the per-layer token counts that achieve these TFLOPs.

Method	VQA ^{v2}	GQA	VizWiz	SQA ^I	Seed ^I	VQA ^{Text}	POPE	MME	MMB	MMB ^{CN}	Rel. Avg.
<i>Upper Bound: 100% TFLOPs (= 2880 Visual Tokens Every Layer)</i>											
LLaVA-NeXT-7B	81.3	62.5	55.2	67.5	70.2	60.3	86.8	1511.8	65.8	57.3	100.0%
<i>Retain 23% TFLOPs (= 640 Visual Tokens Every Layer)</i>											
FastV (Chen et al., 2024)	77.0	58.9	53.9	67.4	62.5	58.1	79.5	1412.6	63.1	53.5	94.6%
PDrop (Xing et al., 2024)	79.1	60.0	53.8	66.7	67.4	57.8	83.8	1475.9	64.1	55.2	96.9%
SparseVLM (Zhang et al., 2024c)	79.2	61.2	53.6	67.6	68.1	59.7	85.3	1456.8	65.9	58.6	98.6%
PruMerge+ (Shang et al., 2024)	78.2	60.8	57.9	67.8	67.7	54.9	85.3	1480.2	64.6	57.3	98.1%
TRIM (Song et al., 2025)	78.3	62.1	54.8	66.9	67.3	54.8	86.9	1471.8	66.8	55.8	97.7%
VisionZip (Yang et al., 2024)	79.1	61.2	57.1	68.1	67.4	59.9	86.0	1493.4	65.8	58.1	99.4%
DART (Wen et al., 2025)	78.3	61.3	57.0	68.2	67.9	59.5	85.0	1450.2	64.9	57.1	98.6%
DivPrune (Alvar et al., 2025)	79.3	61.9	55.7	67.8	68.6	57.0	86.9	1469.7	65.8	57.3	98.8%
VisPruner	79.8	61.6	57.1	69.0	66.2	59.3	85.9	1480.7	65.0	57.3	99.0%
DOP_V (Ours)	80.2	62.1	56.9	68.7	68.2	59.4	87.3	1484.1	66.3	58.7	100.0%
CDPruner (Zhang et al., 2025)	79.9	62.6	55.6	67.9	68.9	58.4	87.3	1474.5	66.3	57.5	99.4%
DOP_{CD} (Ours)	80.3	62.5	55.2	68.2	69.3	59.3	87.6	1477.3	66.6	58.3	99.8%
<i>Retain 14% TFLOPs (= 320 Visual Tokens Every Layer)</i>											
FastV (Chen et al., 2024)	61.5	49.8	51.3	66.6	58.6	52.2	49.5	1099.0	53.4	42.5	80.2%
PDrop (Xing et al., 2024)	66.8	50.4	49.7	66.7	59.7	49.0	60.8	1171.5	55.5	44.7	82.8%
SparseVLM (Zhang et al., 2024c)	74.6	57.9	54.2	67.2	62.3	56.5	76.9	1386.1	63.1	56.7	94.0%
PruMerge+ (Shang et al., 2024)	75.3	58.8	57.7	68.1	63.5	54.0	79.5	1444.3	63.0	55.6	95.2%
TRIM (Song et al., 2025)	74.9	59.9	53.5	66.2	64.3	50.2	86.5	1443.8	63.5	51.0	93.8%
VisionZip (Yang et al., 2024)	76.2	58.9	56.2	67.5	63.4	58.8	82.3	1397.1	63.3	55.6	95.8%
DART (Wen et al., 2025)	75.7	59.5	56.8	67.5	64.8	57.6	81.0	1419.5	64.2	55.7	96.1%
DivPrune (Alvar et al., 2025)	77.2	61.1	55.6	67.7	67.1	56.2	84.7	1423.3	63.9	55.7	96.9%
VisPruner	75.7	58.4	57.0	69.5	62.8	57.6	80.4	1370.1	63.6	55.8	95.5%
DOP_V (Ours)	77.6	60.4	56.4	69.7	65.2	59.2	84.6	1455.7	65.1	57.5	98.2%
CDPruner (Zhang et al., 2025)	78.4	61.6	55.8	67.8	67.3	57.4	87.2	1453.0	65.5	55.7	98.1%
DOP_{CD} (Ours)	79.1	61.7	55.4	68.0	68.4	57.9	87.4	1472.9	66.8	56.9	99.0%
<i>Retain 9% TFLOPs (= 160 Visual Tokens Every Layer)</i>											
PruMerge+ (Shang et al., 2024)	70.5	56.2	57.2	66.9	60.1	50.3	71.1	1289.6	58.0	48.9	88.9%
TRIM (Song et al., 2025)	71.0	57.4	52.9	65.5	61.8	45.8	84.8	1275.8	61.6	45.2	89.1%
VisionZip (Yang et al., 2024)	71.4	55.2	55.5	67.9	58.3	55.0	74.9	1327.8	58.6	50.4	90.3%
DART (Wen et al., 2025)	72.5	56.8	56.7	67.8	60.6	54.9	75.3	1325.4	62.0	53.6	92.3%
DivPrune (Alvar et al., 2025)	75.0	59.3	56.1	67.1	64.9	54.1	80.0	1356.6	62.9	53.7	94.2%
VisPruner	70.6	54.7	57.1	68.6	58.1	56.0	72.7	1226.0	60.5	51.4	90.2%
DOP_V (Ours)	74.1	57.6	56.5	68.7	61.2	57.1	79.4	1355.6	62.1	55.1	94.1%
CDPruner (Zhang et al., 2025)	76.7	60.8	55.2	67.5	65.9	55.4	86.8	1425.3	64.2	53.8	96.3%
DOP_{CD} (Ours)	77.5	61.2	55.1	67.5	66.7	56.7	87.5	1446.4	64.8	55.1	97.2%

Table 10: **Performance comparison of different pruning methods on LLaVA-NeXT-7B (Liu et al., 2024a) under different computation budgets.** We evaluate across 10 benchmarks: We evaluate across 10 benchmarks: VQA^{v2} (Goyal et al., 2017), VizWiz (Gurari et al., 2018), SQA^I (Saikh et al., 2022), GQA (Hudson & Manning, 2019), Seed^I (Li et al., 2023a), MME (Fu et al., 2023), MMB (Liu et al., 2023b), POPE (Li et al., 2023c), MMB^{CN} and VQA^{Text} (Singh et al., 2019). We report accuracy (%) for most benchmarks. Avg. represents the mean performance ratio relative to Vanilla across all benchmarks (higher is better). **Bold** values indicate the best performances in each setting. DOP_V uses VisPruner to reduce visual tokens, while DOP_{CD} uses CDPruner. DOP consistently outperforms all baselines with policies only optimized on a subset of only 100 TextVQA training set samples. Lower Bound indicates the minimum possible computation in our settings. Our comparison matches actual TFLOPs and notes the per-layer token counts that achieve these TFLOPs.

Method	VQA ^{v2}	GQA	VizWiz	SQA ^I	Seed ^I	VQA ^{Text}	POPE	MME	MMB	MMB ^{CN}	Rel. Avg.
<i>Upper Bound: 100% TFLOPs (= 576 Visual Tokens Every Layer)</i>											
LLaVA-NeXT-13B	82.3	64.4	59.1	73.1	71.2	63.2	85.3	1539.5	68.5	61.2	100%
<i>Retain 23% TFLOPs (= 640 Visual Tokens Every Layer)</i>											
FastV (Chen et al., 2024)	79.4	60.9	56.4	71.7	67.5	60.7	80.2	1516.7	65.5	59.9	96.1%
PDrop (Xing et al., 2024)	81.1	62.8	58.1	71.7	69.6	62.1	84.4	1559.1	66.6	60.8	98.5%
SparseVLM (Zhang et al., 2024c)	79.9	62.7	57.5	72.5	69.5	62.8	85.6	1562.7	68.8	64.0	99.5%
PruMerge+ (Shang et al., 2024)	78.7	62.8	56.2	70.6	69.7	56.2	83.7	1497.3	67.4	61.9	96.7%
TRIM (Song et al., 2025)	79.4	63.1	54.1	71.2	69.7	57.6	87.3	1554.6	68.7	61.2	97.6%
VisionZip (Yang et al., 2024)	79.7	62.9	56.2	70.8	69.8	62.1	85.8	1549.2	68.1	62.6	98.6%
DART (Wen et al., 2025)	79.3	62.7	56.2	71.0	69.2	61.3	85.2	1542.4	67.6	61.9	98.0%
DivPrune (Alvar et al., 2025)	80.4	63.5	56.7	72.2	70.1	59.2	86.5	1526.1	67.5	62.9	98.5%
VisPruner (Zhang et al., 2024a)	79.7	63.0	56.7	71.2	68.6	62.0	84.8	1561.2	67.4	62.9	98.4%
DOP_V (Ours)	80.8	63.5	55.3	71.7	70.5	61.2	86.4	1592.2	69.5	62.6	99.3%
CDPruner (Zhang et al., 2025)	81.0	64.0	57.1	71.8	70.6	61.0	86.1	1545.6	68.9	62.1	99.2%
DOP_{CD} (Ours)	81.4	63.9	55.7	72.5	71.2	60.0	86.1	1567.4	69.0	62.5	99.2%
<i>Retain 14% TFLOPs (= 320 Visual Tokens Every Layer)</i>											
FastV (Chen et al., 2024)	69.8	54.6	53.3	70.5	59.9	55.4	63.6	1279.0	59.8	54.4	86.2%
PDrop (Xing et al., 2024)	75.4	57.7	52.1	72.1	63.3	56.2	74.6	1386.3	62.8	55.3	90.5%
SparseVLM (Zhang et al., 2024c)	76.7	60.9	54.7	70.9	66.8	60.0	81.5	1491.6	68.0	63.5	96.2%
PruMerge+ (Shang et al., 2024)	75.9	61.1	53.6	70.7	66.9	55.9	79.1	1426.5	66.6	60.6	93.9%
TRIM (Song et al., 2025)	75.9	61.3	52.2	69.9	67.0	52.8	87.2	1476.6	67.3	57.4	93.9%
VisionZip (Yang et al., 2024)	76.8	60.7	54.8	70.2	66.6	60.7	82.3	1487.3	66.5	62.3	95.8%
DART (Wen et al., 2025)	76.4	60.9	54.2	69.8	66.8	59.7	81.1	1457.4	65.9	61.9	95.0%
DivPrune (Alvar et al., 2025)	78.1	61.8	55.0	72.3	67.8	57.6	85.2	1473.0	65.9	61.9	96.2%
VisPruner (Zhang et al., 2024a)	76.7	60.6	54.4	70.1	65.1	60.5	81.7	1523.6	66.2	62.3	95.6%
DOP_V (Ours)	78.6	61.7	54.7	71.1	67.5	61.3	84.3	1544.7	67.2	62.4	97.2%
CDPruner (Zhang et al., 2025)	79.6	63.1	55.1	71.6	68.9	58.7	87.6	1498.5	66.3	61.8	97.3%
DOP_{CD} (Ours)	80.2	63.1	54.5	71.5	69.9	59.5	87.6	1548.2	67.7	62.8	98.2%
<i>Retain 9% TFLOPs (= 160 Visual Tokens Every Layer)</i>											
PruMerge+ (Shang et al., 2024)	71.6	57.9	50.8	70.1	62.5	52.8	72.1	1345.9	63.2	57.1	88.8%
TRIM (Song et al., 2025)	72.1	58.9	51.2	69.1	63.4	49.2	87.0	1392.3	65.7	51.6	90.0%
VisionZip (Yang et al., 2024)	72.4	57.8	52.5	69.7	62.4	58.6	76.8	1393.9	64.8	60.0	91.5%
DART (Wen et al., 2025)	72.8	58.7	52.1	70.1	63.5	57.2	75.7	1389.3	64.6	60.8	91.6%
DivPrune (Alvar et al., 2025)	75.6	60.0	53.5	71.4	64.9	56.3	81.9	1436.7	65.1	60.9	93.7%
VisPruner (Zhang et al., 2024a)	72.4	57.7	52.2	70.9	61.1	58.3	76.6	1397.0	63.4	60.2	91.2%
DOP_V (Ours)	75.1	59.3	52.7	70.7	63.6	59.5	79.7	1467.4	65.7	61.5	93.8%
CDPruner (Zhang et al., 2025)	77.8	62.2	53.1	71.7	67.1	56.7	88.3	1476.9	65.9	60.1	95.7%
DOP_{CD} (Ours)	78.8	62.6	52.6	71.8	68.2	57.7	88.1	1504.1	66.7	62.2	96.7%

Table 11: **Performance on LLaVA-NeXT-13B (Liu et al., 2024a) under different computation budgets.** We evaluate across 10 benchmarks: VQA^{v2} (Goyal et al., 2017), VizWiz (Gurari et al., 2018), SQA^I (Saikh et al., 2022), GQA (Hudson & Manning, 2019), Seed^I (Li et al., 2023a), MME (Fu et al., 2023), MMB (Liu et al., 2023b), POPE (Li et al., 2023c), MMB^{CN} and VQA^{Text} (Singh et al., 2019). We report accuracy (%) for most benchmarks. Avg. represents the mean performance ratio relative to Vanilla across all benchmarks (higher is better). **Bold** values indicate the best performances in each setting. DOP_V uses VisPruner to reduce visual tokens, while DOP_{CD} uses CDPruner. DOP consistently outperforms all baselines with policies only optimized on a subset of only 100 TextVQA training set samples. Lower Bound indicates the minimum possible computation in our settings. Our comparison matches actual TFLOPs and notes the per-layer token counts that achieve these TFLOPs.

Method	TextVQA	ChartQA	AI2D	OCRBench	MME	MMB-EN	MMB-CN	Rel. Avg.
<i>Upper Bound: 100% TFLOPS (= 1296 Visual Tokens Every Layer)</i>								
Qwen2.5-VL-7B	85.5	86.5	81.0	879	2286	80.2	82.7	100.0%
<i>Retain 43% TFLOPS (= 512 Visual Tokens Every Layer)</i>								
FastV (Chen et al., 2024)	84.1	82.2	78.8	815	2317	82.0	81.8	98.0%
DivPrune (Alvar et al., 2025)	81.8	79.6	78.6	800	2279	81.6	82.1	96.6%
CDPruner (Zhang et al., 2025)	84.2	82.8	78.9	827	2327	82.2	82.6	98.5%
Resizing	81.8	85.8	80.8	856	2351	79.8	82.6	99.1%
DOP_R (Ours)	82.2	85.8	80.8	868	2355	80.1	82.6	99.5%
<i>Retain 26% TFLOPS (= 256 Visual Tokens Every Layer)</i>								
FastV (Chen et al., 2024)	81.5	70.9	76.2	703	2238	79.6	78.9	92.0%
DivPrune (Alvar et al., 2025)	76.0	65.1	76.5	692	2184	80.0	79.6	89.8%
CDPruner (Zhang et al., 2025)	82.4	73.0	77.5	749	2245	80.9	79.9	93.9%
Resizing	76.6	82.5	79.9	813	2346	80.0	81.7	96.7%
DOP_R (Ours)	79.8	83.1	79.8	828	2351	79.7	82.4	97.7%
<i>Retain 16% TFLOPS (= 128 Visual Tokens Every Layer)</i>								
FastV (Chen et al., 2024)	73.8	52.2	71.4	531	2008	72.9	72.2	80.2%
DivPrune (Alvar et al., 2025)	67.0	50.4	72.1	549	2108	77.8	77.8	81.6%
CDPruner (Zhang et al., 2025)	77.8	59.2	74.0	632	2127	76.2	76.5	86.2%
Resizing	67.0	61.8	78.5	728	2322	79.3	81.3	89.7%
DOP_R (Ours)	69.9	70.8	79.1	741	2303	79.9	81.5	92.1%

Table 12: **Performance comparison on Qwen2.5-VL-7B under different computation budgets.** We evaluate across 7 benchmarks: TextVQA, ChartQA, AI2D, OCRBench, MME, MMB-EN, and MMB-CN. **Rel. Avg.** is the mean performance ratio relative to the full model.

Method	TextVQA	ChartQA	AI2D	OCRBench	MME	MMB-EN	MMB-CN	Rel. Avg.
<i>Upper Bound: All 1280 Tokens (100%)</i>								
InternVL3-8B	81.5	85.1	85.2	853	2394	83.9	82.6	100.0%
<i>Retain 27% TFLOPs (= 256 Visual Tokens Every Layer)</i>								
FastV (Chen et al., 2024)	74.4	70.7	82.2	632	2348	83.6	82.0	91.7%
DivPrune (Alvar et al., 2025)	64.7	57.5	80.9	477	2249	80.8	80.2	83.6%
CDPruner (Zhang et al., 2025)	75.7	72.0	82.7	640	2334	83.5	81.7	92.2%
Resizing	70.3	75.0	84.1	743	2369	84.4	85.0	94.7%
DOP_R (Ours)	71.9	74.4	85.1	732	2339	85.3	86.1	95.0%
<i>Retain 18% TFLOPs (= 128 Visual Tokens Every Layer)</i>								
FastV (Chen et al., 2024)	63.7	46.9	77.3	426	2250	81.3	80.2	80.3%
DivPrune (Alvar et al., 2025)	55.6	42.7	76.4	378	2166	78.4	77.6	75.8%
CDPruner (Zhang et al., 2025)	67.5	50.8	79.9	471	2282	82.1	80.3	83.1%
Resizing	57.6	49.0	82.0	573	2301	82.5	82.5	83.7%
DOP_R (Ours)	64.6	60.9	83.5	659	2354	84.8	84.9	89.8%

Table 13: **Performance comparison on InternVL3-8B under different computation budgets.** We evaluate across 7 benchmarks (TextVQA, ChartQA, AI2D, OCRBench, MME, MMB-EN, MMB-CN). **Rel. Avg.** denotes the mean performance ratio relative to the original model. **Bold** indicates the best result within each budget.

E.4 FULL OPTIMIZATION COST

In Table 14, we present the optimization cost of DOP on LLaVA-1.5-7B&13B, LLaVA-Next-7B&13B, Qwen2.5-VL-7B, and InternVL3-8B using the same 100 TextVQA samples as the validation set. Since other computational costs are negligible compared to the validation runs for divergence evaluation, we primarily report the time required to complete divergence evaluation across all sampled points. Note that as mentioned in Section C.2, we only need to generate the first output token for each sample to compute the divergence, eliminating the need to generate complete ques-

⁴<https://docs.scipy.org/doc/scipy/reference/generated/scipy.stats.spearmanr.html>

Model	LLaVA-1.5	LLaVA-Next	Qwen2.5-VL	InternVL3
Size	7B / 13B	7B / 13B	7B	8B
Cost (min)	5 / 7	12 / 18	10	7

Table 14: Optimization cost (minutes) on a single NVIDIA A100-80G GPU across different models. This cost represents the one-time expense to evaluate sampled individual divergences on 100 TextVQA samples (note that we only need to generate the first token for each sample). Subsequently, solving optimization for different TFLOPs ratios to obtain policies requires only negligible CPU operations.

TFLOPs	LLaVA-1.5-7B				LLaVA-1.5-13B				LLaVA-Next-7B				LLaVA-Next-13B			
	100%	37%	28%	23%	100%	37%	28%	23%	100%	23%	14%	9%	100%	23%	14%	9%
d_A	32	25	26	25	40	40	40	31	32	25	29	30	40	340	38	38
d_P	32	19	19	16	40	20	21	16	32	16	16	16	40	19	20	20
n_v	576	192	97	51	576	192	96	58	2880	965	485	240	2880	960	480	240

Table 15: **DOP policies for all LLaVA models across TFLOPs ratios.** Rows list MHA depth (d_A), MLP depth (d_P), and visual token count (n_v). For each model, the 100% TFLOPs configuration corresponds to d_A and d_P equal to the number of decoder layers, and n_v equal to the original visual token count. The policies shown are for DOP_{CD}, while DOP_V policies are basically identical.

tion responses. The results demonstrate that our DOP is highly efficient, with optimization costs not exceeding 18 minutes on a single NVIDIA A100-80G GPU across all models. According to Section F.1, by using 25 samples for optimization, we can further reduce the optimization cost to as low as 2 minutes with comparable performance, though we default to using 100 TextVQA samples in our main experiments since this configuration is already sufficiently efficient.

E.5 ALL DOP POLICIES

DOP policies for LLaVA-series models across different TFLOPs ratios are presented in Table 15, while policies for Qwen2.5-VL and InternVL3 are shown in Table 16.

F ADDITIONAL ABLATION

F.1 OPTIMIZATION EFFICIENCY ABLATION

Table 17 shows the performance and optimization cost with different numbers of optimization samples on LLaVA-1.5-7B at 28% TFLOPs. The results show minimal performance differences across 25-500 samples, with only 10 samples causing substantial degradation while still outperforming CDPruner. This validates our default 100 samples setting and shows we can reduce to 25 samples to reduce time cost to 2 minutes with comparable performance, though we default to using 100 TextVQA samples in our main experiments since this configuration is already sufficiently efficient.

F.2 DIVERGENCE VISUALIZATION

In Figure 4, we present individual divergences evaluated on different benchmarks with respect to MHA depth, MLP depth, and visual token count. We observe that on SeedBench, pruning MHA and MLP visual operations after half of the layers causes virtually no divergence, whereas TextVQA and VQAv2 only exhibit small divergence after the 26th layer. This phenomenon may be attributed to SeedBench’s multiple-choice instruction format, where answers are embedded within the text, allowing the model to accomplish the task using only shallow visual operations.

Note that the absolute values of divergences across different tasks are not directly comparable due to variations in data characteristics and task formats. For instance, higher divergence values on VQAv2 compared to TextVQA do not imply that VQAv2 is more sensitive to pruning; only divergences within the same task can be meaningfully compared.

TFLOPs	Qwen2.5-VL-7B				InternVL3-8B		
	100%	43%	26%	16%	100%	27%	18%
d_A	28	28	28	28	28	28	28
d_P	28	20	16	17	28	17	19
n_v	1296	640	384	165	1280	361	169

Table 16: **DOP policies for Qwen2.5-VL-7B and InternVL3-8B across TFLOPs ratios.** Rows list MHA depth (d_A), MLP depth (d_P), and visual token count (n_v), where 100% TFLOPs corresponds to $d_A = d_P =$ number of decoder layers and $n_v =$ original visual token count.

#Samples	10	25	50	100	200	500	CDPruner
Cost (min)	1	2	3	5	10	24	-
Rel. Avg.	97.0%	97.7%	97.3%	97.9%	97.6%	97.5%	96.7%

Table 17: **Optimization Efficiency Ablation.** Performance of LLaVA-1.5-7B with different numbers of samples for optimization, showing optimization cost on a single NVIDIA A100-80G GPU and relative performance when retaining 28% TFLOPs across the same benchmarks as Table 8. Optimization with 25 to 500 samples shows minimal performance differences.

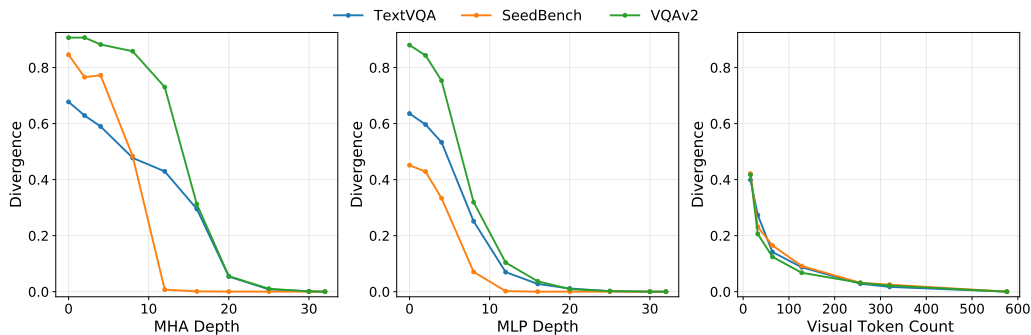


Figure 4: Individual divergence patterns across different benchmarks on LLaVA-1.5-7B. We visualize the three individual divergences $\hat{D}_A(d_A)$, $\hat{D}_P(d_P)$, and $\hat{D}_v(n_v)$ with respect to MHA depth, MLP depth, and visual token count respectively. Each subplot shows divergences evaluated on three benchmarks, including TextVQA (blue), VQAv2 (green), and SeedBench (orange). Notably, SeedBench exhibits significantly higher redundancy in deeper layer operations compared to the other two benchmarks.